International Journal of Mass Spectrometry 305 (2011) 1–19

Contents lists available at ScienceDirect

International Journal of Mass Spectrometry

journal homepage: www.elsevier.com/locate/ijms

Review

Magnetic resonance and radio frequency mass spectrometers and their application

N.N. Aruev*

Ioffe Physico-Technical Institute of the Russian Academy of Sciences, Polytekhnicheskaya Street 26, 194021 St. Petersburg, Russian Federation

ARTICLE INFO

Article history:
Received 2 February 2011
Received in revised form 11 May 2011
Accepted 13 May 2011
Available online 19 May 2011

PACS:
82.80.Qx

Keywords:
Cyclotron frequency
Resolving power
Sensitivity
Dispersion
Magnetic field homogeneity

ABSTRACT

Development of magnetic resonance mass spectrometers (MRMSs) was started at the Leningrad Physico-Technical Institute as far back as the early 1950s, and work on their upgrading and refinement is still in progress. For more than 50 years, the activities in the area of their modification and potential applications have been charged by Boris Aleksandrovich Mamyrin (May 25, 1919–March 05, 2006), assisted by followers and colleagues. Altogether, 7 such instruments have been built, and 5 of them still remain at the Ioffe Institute, with only two of them being actively in use. At about the same time, Lincoln Gilmore Smith (February 12, 1912–December 9, 1972) was developing and building together with colleagues a mass synchrometer at the Brookhaven National Laboratory and, subsequently, a radio frequency mass spectrometer (RFMS) at Princeton University. After the death of L.G. Smith, the unique instrument did not find proper application in the USA and was moved to Delft University of Technology, where it likewise did not enjoy much use for many years. The principle underlying the operation of both instruments, MRMS and RFMS, is based essentially on the cyclotron frequency of ion motion in a circular orbit in a homogeneous magnetic field being dependent on the field strength and the ion mass to charge ratio only. The specific principle of operation employed confers extremely high analytical characteristics to these mass spectrometers. (Fourier-transform ion-cyclotron-resonance mass spectrometers have a radically different design and are not considered here.) Indeed, the resolving power of one of the MRMSs is as high as ~350,000 at half-maximum of the mass peak, the absolute sensitivities of other instruments amount to ~30,000 atoms in a mass analyzer (1–3) l in volume under static pumping, with the dynamic range reaching 10^{11} (for instance, in studies of the $^3He/^4He$ isotope ratio). These instruments enjoyed widespread use in studies of the isotopes of helium and of other noble gases in natural and technogenic samples, as well as in precision measurements of fundamental physical constants, in particular, of the magnetic moment of the proton in nuclear magnetons and of the tritium half-life. As for the RFMS, its resolving power reached as high as ~400,000 in atomic mass measurements. The unique peak matching technique developed by L.G. Smith permitted one to locate the center of a mass line to within 1/2500 fraction of its width, thus offering a possibility of conducting measurements of cyclotron frequencies and, hence, of atomic masses with a relative uncertainty of $\sim 10^{-9}$. It is the danger of these unique instruments sinking into oblivion that has motivated our writing of this review paper.

Contents

* Tel.: +7 812 292 7116; fax: +7 812 297 1017.
E-mail address: aruev.mass@mail.ioffe.ru

1387-3806/$ – see front matter © 2011 Elsevier B.V. All rights reserved.
doi:10.1016/j.ijms.2011.05.007

1. Introduction

By definition, the cyclotron frequency of an ion with charge Ze and mass M in a homogeneous magnetic field with strength H is

$$\omega_C = \frac{ZeH}{cM}, \tag{1}$$

where c is the velocity of light. Significantly, magnetic field provides perfect focusing of the ions both in time and space. The period of ion revolution over a circular orbit does not depend on the energy of ions and the angle at which they exit the source, and is given by the relation:

$$T_C = \frac{2\pi Mc}{ZeH}, \tag{2}$$

or, for singly charged ions:

$$T_C \approx 652\frac{M}{H}, \tag{2a}$$

where T_C is in microseconds, M in atomic mass units u, and H is in oersteds.

It is probably the publication by Bleakney and Hipple as far back as 1938 [1] that was the first to put forward an original proposal to use for determination of atomic mass measurements of the time taken by an ion to make a circular turn in a magnetic field; it did not, however, enjoy the publicity it certainly deserved. About 10 years later, soon after the end of the World War 2, mass spectrometry, one of the most accurate methods to study the composition of matter, revealed explosive growth, and three groups of scientists, in the USSR and USA [2–4], proposed, nearly simultaneously, independent methods of determination of atomic masses by measuring cyclotron periods. The work of Fiks [2], then a student of the Leningrad Polytechnic Institute, was continued and expanded in scope in a laboratory of the Ioffe Institute, which was engaged at the time in research along the lines of the Atomic Project. Rather than delving into the design and operation of magnetic time-of-flight mass spectrometers, I am going to dwell, necessarily briefly, on the main stages they passed in their development.

2. First cyclotron instruments

In the instrument built by Goudsmit et al. [3,5] which was called "chronotron", ions are ejected by a short electric pulse from the source, move in a magnetic field of ~450 G over a helicoidal trajectory and make up to 7 complete turns. In the course of this motion, the ions are being separated in mass in accordance with their time of flight, i.e., the cyclotron period. Light ions are the first to reach the collector, and heavy ones, the last. The resolving power of the instrument can be expressed in the following way:

$$R = \frac{M}{\Delta M} = \frac{nT_C}{\Delta t}, \tag{3}$$

where M_1 and M_2 are the masses of two species of ions, $M = (M_1 + M_2)/2 \approx M_1 \approx M_2$, $\Delta M = M_2 - M_1$, n is the number of turns an ion makes in the magnetic field, and Δt is the length in time of the bunch of ions of one mass, which is determined primarily by the width of the ionization region in the ion source. By measuring the difference between the times of flight of ion bunches of different masses, the authors were able to attain a resolving power of the chronotron of 2000–4000, and determined the masses of a number of ions with an uncertainty of $\sim 10^{-3}$ u. This arrangement did not, however, enjoy further development because of the difficulties encountered in reaching a high magnetic field homogeneity in a large volume, with the magnet poles separated by 0.12 m.

Fiks et al. [6] considered three designs of time-of-flight magnetic instruments that were successively built and studied at the Physico-Technical Institute. In the first arrangement, the ions were ejected from a pulsed source in short bunches, separated in time as they moved in a circular trajectory, struck the collector and triggered a gated-sweep oscilloscope. The resolving power of this model was high enough to completely separate the mass lines of the $^{85}Rb^+$ and $^{87}Rb^+$ isotopes, but the ion current intensity was too low to allow reliable studies. In the second arrangement (Fig. 1), an "ion valve" consisting of two grids was introduced at the entrance to the collector. Grid 1 was grounded, while to the second grid electrode one could apply a positive retarding potential E and a pulsed voltage U, which could reduce the potential E and was synchronized with the ejecting pulse of the ion source. If the time of a complete ion turn in the magnetic field coincided with the pulse repetition period, the ions crossed grid 2 and struck collector 3, to be subsequently recorded by the electrometric amplifier. This instrument provided a resolving power of about 500–600, but further improvement of the resolving power by increasing the number of turns of ions in the magnetic field in this arrangement proved to be impossible.

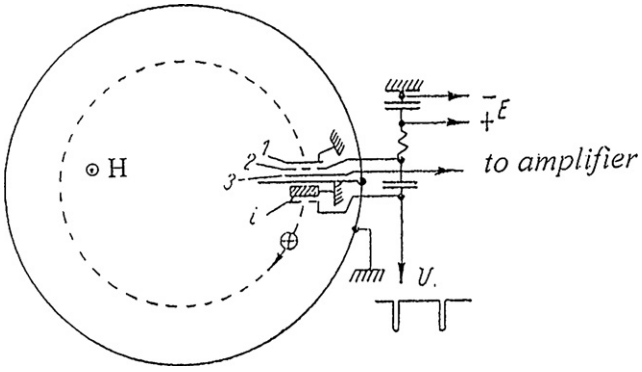

Fig. 1. Scheme of a cyclotron instrument with ion shutter [6]. *i*: ion source, 1: grounded grid, 2: potential electrode, and 3: ion collector.

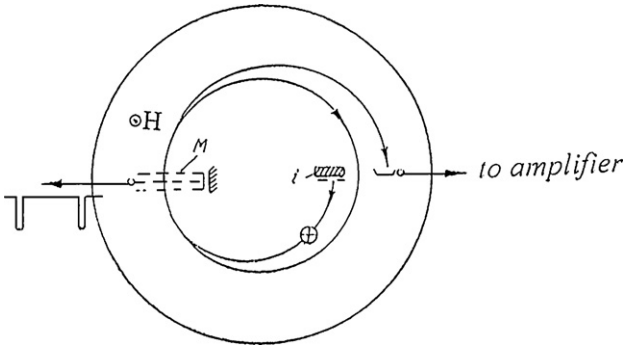

Fig. 2. Ion orbit in a cyclotron instrument [6]: *i*: ion source and M: modulator.

The third model of the time-of-flight instrument based on measurement of ion masses from their cyclotron frequency is shown schematically in Fig. 2.

The ions forming in the ion source make half a turn in the magnetic field and enter a three-grid modulator. The outer grids of the modulator are grounded, and to the second grid is applied a pulsed voltage with a pulse repetition frequency ω and length Δt. In crossing the modulator, the ions receive acceleration with the corresponding increase of the radius of their turn, turn round the source and enter the modulator again. If the pulse repetition frequency ω is proportional to the ion cyclotron frequency ω_c, i.e., $\omega = n\omega_c$, where n is an integer or the number of the modulating voltage harmonic, ions can make several turns in the magnetic field, reach the collector and be detected. It was shown [6] that the expression for the resolving power (3) converts to:

$$R = \frac{M}{\Delta M} = \frac{\omega}{\Delta\omega}, \tag{3a}$$

where $\Delta\omega$ is the width of the mass peak at a preset height. A study of the $^{85}Rb^+$–$^{87}Rb^+$ doublet performed with $n = 3$ demonstrated a resolving power at half-maximum of the mass line of ~1200 [6]. An analysis of the operation of the third model of the instrument offered a number of conclusions: (1) by using high harmonics of the modulating voltage ($n \gg 1$), one can increase substantially the output current of the instrument and, hence, its sensitivity and (2) measurements of ion masses reduce actually to those of frequencies.

3. Mass synchrometer

At about the same time, at the Brookhaven laboratory L.G. Smith proposed a new arrangement for a magnetic time-of-flight mass spectrometer [7], in which an ion moved along a helicoidal trajectory of a decreasing radius.

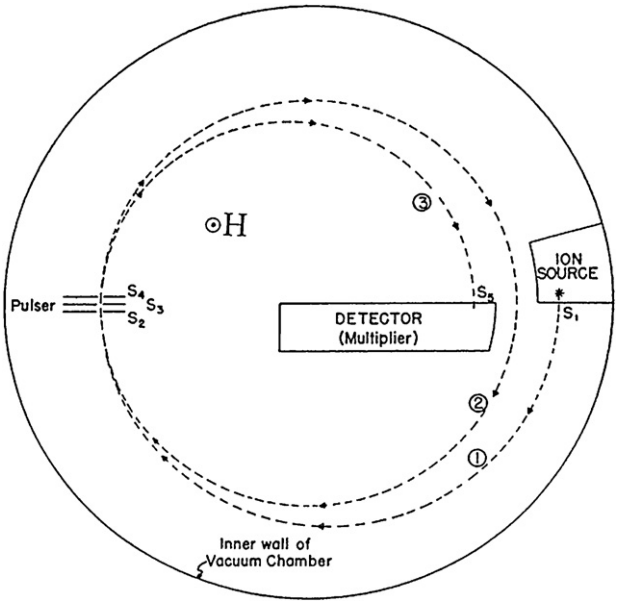

Fig. 3. Schematic cross section of the first mass synchrometer [4]: 1: ion source orbit, 2: drift orbit after the first deceleration of ions, and 3: exit orbit of ions after the second deceleration. S_1: exit slit of ion source, S_2, S_3, S_4: slits of modulator electrodes, and S_5: input slit of detector.

Fig. 3 displays the diagram of the instrument called by its designer "synchrometer". Just as in the preceding instrument, the ions produced in the source make half a turn in the magnetic field and enter a modulator consisting of three parallel plane electrodes with slits S_2, S_3, and S_4. The outer electrodes are grounded, and to the central electrode rectangular pulses that can slow down the ions are applied. The decelerated ions move in an orbit of the smaller radius, turn around the source on its inner side and again enter the modulator. If the time between the pulses applied to the central electrode of the modulator is a multiple of the cyclotron period of ions of a given mass, the ions will again undergo deceleration, pass one half-turn more and fall on the detector, which was based on a plane-dynode photomultiplier to operate in a magnetic field and developed by the author specifically for this instrument [8]. For an orbit diameter of ~0.254 m (between two ion transits of the modulator) and a magnetic field of 820 Oe, ions with $M = 18$, 28, and 44 atomic mass units (u) made, accordingly, 70, 40, and 25 turns in the magnetic field in the time between two voltage pulses applied to the central electrode of the modulator. In this case, the resolving power of the mass synchrometer was estimated from Eq. (3) and was found to be $(8.5–3) \times 10^3$ for ions of different types.

The first reports of modifications introduced into the mass synchrometer design appeared in Ref. [9], with a full description of the new instrument and its theory published subsequently [10]. In contrast to the first model, the ion source in this mass synchrometer operated in continuous mode, with a high-frequency sinusoidal voltage used for modulation for the first time in world practice. To prevent background current and satellite peaks from appearing in the spectra, the authors increased the number of turns of the spiral of decreasing radius to three, and introduced baffles with aperture slits (Fig. 4). Ions exiting the source make a half-turn in the magnetic field and enter the slit modulator S_2–S_3–S_4, where they are acted upon by a decelerating electric field of a high frequency equal to the multiple of the ion cyclotron frequency. The modulated beam of ions makes the following half-turn, and slit S_5 cuts out from each sine period two short bunches of ions, which pass again into the modulator a half-turn later. If the frequency and phase of the modulating voltage applied to the central electrode have been chosen correctly, the ion bunches will undergo two more decelerations,

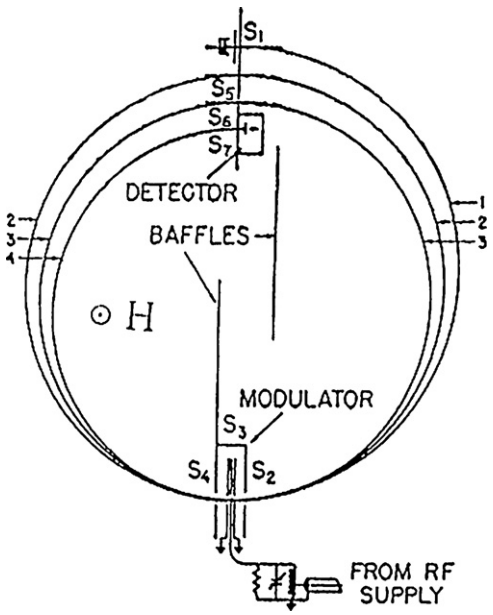

Fig. 4. Scheme of the second mass synchrometer [10]: 1, 2, 3: ion orbits after first, second and third decelerations, S_1: exit slit of ion source, S_2, S_3, S_4: slits of modulator electrodes, S_5, S_6: aperture slits, and S_7: input slit of detector.

until on passing through slits S_6 and S_7, they will impinge on the detector.

Smith and Damm [10] developed an extensive theory describing ion motion in the instrument, which makes it possible to include into consideration geometric, electric, and phase parameters, among them ion orbit motion diameters, widths of the aperture slits and gaps in the modulator, amplitudes of the accelerating and modulating voltages, phase of the high-frequency voltage and its variation during the time ions make a turn in the trajectory, etc. To cite an example, from the expression coupling the radius of rotation of a charged particle with its mass to charge ratio M/q in a constant magnetic field H, which is acted upon by an electric potential U:

$$\rho = \frac{(2UM/q)^{1/2}}{H}. \tag{4}$$

One immediately derives the relation between ρ and the accelerating voltage in the ion source. For rough calculations, one takes usually the common expression $\rho = 144(UM/q)^{1/2}/H$, where the radius ρ is measured in [cm], the accelerating voltage U in [V], ion mass M in atomic mass units [u], ion charge in elementary charges [e], and magnetic field in [Oe]. As can be inferred from Eq. (4), for ions with the same charge in a static MRMS or RFMS stage, as well as in static magnetic mass spectrometers with rigorously set ion motion trajectories, one can write:

$$UM = \text{const}. \tag{5}$$

This relation underpins Bleakney's theorem [11] and the peak-matching method, which are employed successfully in atomic mass measurements performed with static magnetic mass spectrometers.

3.1. Acceleration of ions in the modulator and Bennett's condition

A result of paramount importance that produced a major impact on development of magnetic resonance instruments was obtained by L.G. Smith in his consideration of the process of ion acceleration in a two-gap symmetric modulator consisting of three plane grid electrodes. The outer electrodes are grounded and are at a distance a from the central electrode, to which a high-frequency sine voltage $U_m \sin \omega t$ is applied. Ions entering the modulator with a velocity v_0 are accelerated by the voltage by an increment Δv, which in a first approximation depends harmonically on the time the ion entered the modulator. This dependence may be considered as a function Δv of the phase φ of the modulator voltage, which can be identified with the instant of passage by the ions of the central modulator grid. The analysis conducted in Ref. [10] yielded the same result as obtained by Bennett [12] for the case of acceleration of an ion beam moving in a straight line by a sine voltage applied to the central grid of the double-gap modulator. In this case:

$$\Delta v = \frac{U_m \cos\varphi(1 - \cos\theta)}{\theta}, \tag{6}$$

where

$$\theta = \frac{a\omega}{v_0}, \tag{7}$$

and U_m and ω are the amplitude of the modulating voltage and its angular frequency, respectively, and a is the modulator grid separation. It was shown [12] that the factor $(1 - \cos\theta)/\theta$ has a maximum at the transit angle:

$$\theta \approx \frac{3\pi}{4}. \tag{8}$$

We see that ions acquire the maximum increment of the velocity and, hence, of the radius of motion if a and ω in Eq. (7) are chosen such that the phase angle of the high-frequency modulating voltage changes during the passage through the modulator by $3\pi/4$. Eqs. (6) and (7) relate the electrical, frequency, and phase parameters of resonance instruments and are used to advantage in calculation of their analytical characteristics. As it turned out later on, the condition of W.H. Bennett, Jr. is applicable also to the double-gap symmetric slit modulator, the only difference being that in this case a is not the distance between the central and the outer modulator electrodes but rather an effective quantity allowing for the electric field distortion in the electrode slit.

The theory of L.G. Smith provided a possibility of calculating the resolving power and intensity of synchrometer peaks. The resolving power calculations were found to correspond good enough with experiment, but the calculated number of the high-frequency harmonic ($n = 138$) differed noticeably from the experimental value ($n = 103$). The measured value of the amplitude of modulator voltage applied to the central electrode of the modulator was also substantially in excess of the calculated value. The authors believed the most serious drawback of their mass synchrometer to be its low sensitivity compared, for instance, with magnetic static mass spectrometers, and even questioned the possibility of their potential to become truly analytic instruments. L.G. Smith having been an internationally recognized authority in the mass-spectrometer research community, these comments could produce a negative impact on further development and progress in the field of radio frequency mass spectrometry.

The highest resolving power reached with mass synchrometer, which for various ions was $(10–25) \times 10^3$, as well as the peak matching technique developed at that time and permitting determination of the centers of mass peaks in units of frequency to within 1/2000 part, provided a possibility of conducting precision measurements of atomic masses [13] with an uncertainty of ~0.01 ppm. Further improvement of the resolving power and sensitivity of the mass synchrometer appeared questionable, and L.G. Smith proposed an original design of a resonance mass spectrometer [14] and, soon thereafter, started construction of a novel magnetic cyclotron instrument at Princeton, which lasted 7 long years.

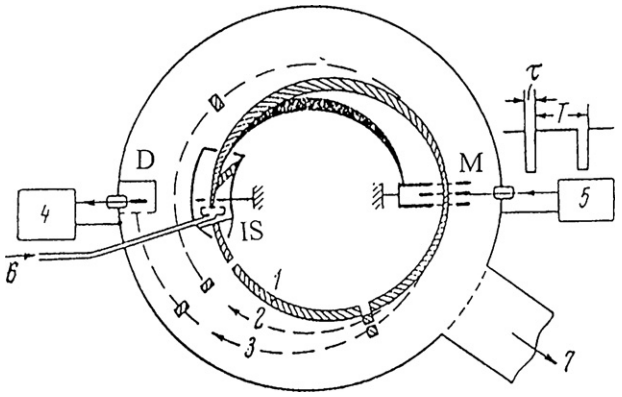

Fig. 5. Design schematic of the pulse magnetic resonance mass spectrometer [15]: IS: ion source, M: modulator, D: detector, 1: orbit of ion source, 2: drift orbit and ion bunches on it, 3: exit orbit and ion bunches, 4: tube electrometer, 5: pulse generator, 6: gas inlet, and 7: vacuum pump.

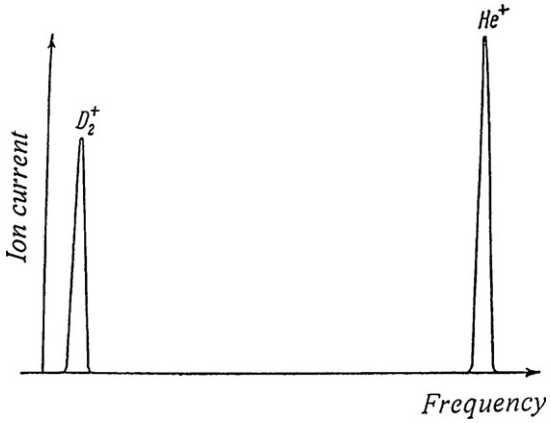

Fig. 6. Mass spectrum of $^2D_2{}^+$–$^4He^+$ doublet [15].

4. Pulsed magnetic resonance mass spectrometer

The studies of various arrangements of resonance mass spectrometers conducted at the time at the Leningrad Physico-Technical Institute were aimed at development of an analytic instrument with a high resolving power and high sensitivity, which was needed for research in the field of gas dynamics. The first operational instrument (Fig. 5) [15] was actually a realization of the arrangement described in Ref. [6]. Its principle of operation having been treated above briefly and here we are going to dwell on some details and the factors affecting the sensitivity of such instruments. Compared with magnetic static mass spectrometers, the sensitivity of pulsed instruments drops sharply because the current to the detector flows during short periods of time only, and is absent during the intervals between the pulses. The aperture ratio and the sensitivity of a pulsed MRMS fall off also as an ion bunch traverses the three modulator grids. The more turns makes an ion bunch in the drift orbit (2 in Fig. 5) between the first and second acceleration in the modulator (n = 1–5), the higher the resolving power and the lower the aperture ratio and sensitivity of the instrument. Apart from this, the output ion current may decrease noticeably as a result of the ion beam being affected by stray electric fields generated by surface charges and contact potential differences at the inner screens, diaphragms, and other elements of the vacuum chamber.

The MRMS resolving power is determined by the duration of ion bunches, i.e., their length in the direction of motion. In turn the duration of ion bunches is determined by the dimension of accelerating modulator gap and duration of generator pulse τ. These circumstances enable to use wide slits in the ion source and all diaphragms, up to a few mm, and in way increase noticeably the operating current and sensitivity of the instrument without compromising markedly the resolving power. Interestingly, the slits used in static mass spectrometers to obtain $R \sim (5–10) \times 10^3$ are a few tens of μm wide, i.e., hundreds of times more narrow than those in resonance instruments. To increase the ion source current efficiency and enhance the sensitivity of the pulsed MRMS being discussed here, the ionization chamber operated in the ion accumulation mode between the ejector pulses which were matched through a delay line with the pulses at the modulator. As a result, the source produced ions in a pulsed mode, but the current density in a pulse increased T/τ_1 times (here T is the repetition frequency of voltage pulses applied to the source and modulator, and τ_1 is the length of the ion bunch, which is determined primarily by the width of the source ionization chamber [15]. To bring to a minimum the deleterious effect of stray electric fields on ion motion and instrument sensitivity, additional copper baffles, either polished or gold-plated, were provided, and evacuation was performed only through liquid nitrogen traps to prevent oil vapors from getting into the analyzer.

The pulsed MRMS instrument designed in this way had the following characteristics. A permanent magnet with pole pieces 220 mm in diameter and a gap of ~40 mm generates a magnetic field $H \approx 800$ Oe. The brass nonmagnetic vacuum chamber was 170 mm wide inside and ~26 mm high. The ion energy at source exit was ~200 eV. The source and modulator pulse repetition frequency could be varied in the 300–800 kHz range, and the modulation pulse length was ~0.007 μs long. The pulse voltage was adjustable from 0 to 250 V. For the instrument resolving power of 4–5 thousand at half-maximum of the mass line, the output ion current was $\sim 10^{-11}$ A. Among the significant advantages of the instrument the authors pointed out the absence of tails at the foot of the peaks. Fig. 6 displays a mass spectrum of the doublet $^2D^+{}_2$–$^4He^+$ (mass difference ΔM = 0.0256 u) obtained with a pulsed MRMS.

The main drawbacks of this mass spectrometer were: (1) in order to reach a high resolving power, one had to operate with ions making a large number of turns in the drift orbit (n = 3–5), which reduced the output current and the sensitivity and (2) the presence of harmonics, i.e., the possibility for peaks of the same mass number to appear at different repetition frequencies of the pulses applied to the modulator and the ion source.

5. Modes and theoretical consideration of the MRMS operation

To overcome these disadvantages, a novel arrangement of the pulsed MRMS was proposed at the Physico-Technical Institute [16], in which a trapezoidal periodic voltage is applied to the modulator, and the ion source operates in a continuous mode. Ions entering the modulator during the pulse undergo acceleration and their orbit grows in diameter. Fig. 7 presents the diagram of this instrument and Fig. 8 illustrates the modulation of the energy of ions for different times of their arrival to the modulator. We start by assuming that the modulator pulse is symmetric in shape, and that the leading and trailing edges of the pulse are linear, with the same rise and decay times. The ions whose energy has increased in the modulator in the interval from ΔE_1 to ΔE_2 will pass slit S_2 (Fig. 7) to form two ion bunches, (1–2) and (3–4) (Fig. 8). The ions with the maximum energy increment ΔE_U should not pass the exit slit S_3. If, however, $\Delta E_U > \Delta E_3$, and ions do pass the exit slit S_3 after the first acceleration, direct ejection is effected, a mode which permits adjustment of the ion source and detection system to optimum operation.

The ion bunches cut out by slit S_2 move in the drift orbit and enter again the modulator after a half-turn. Depending on the actual

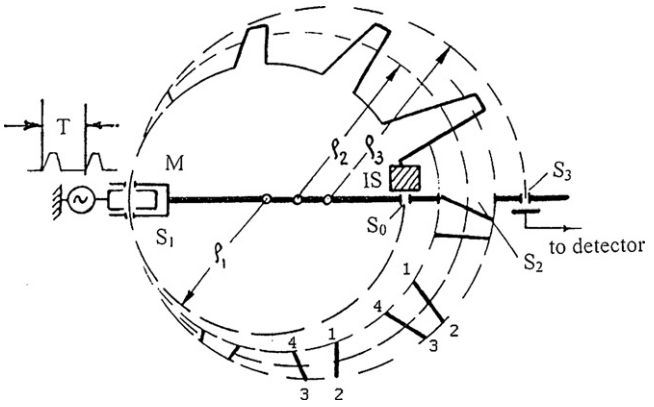

Fig. 7. Scheme of MRMS with trapezoidal modulating potential [16]: IS: ion source, M: modulator, S_0: exit slit of ion source, S_1: modulator slits, S_2: drift slit, S_3: detector slit, ρ_1: radius of the ion source orbit, ρ_2: radius of the drift orbit, ρ_3: radius of the exit orbit, 1–2 and 3–4: ion bunches are cut by S_2 from modulated ion beam.

ratio of the cyclotron period T_C to the generator pulse repetition frequency T, ions can become accelerated once more, reach the exit slit, and become properly detected. Several cases may be envisaged here.

5.1. First compensation mode

$$T = T_C - t_1. \tag{9}$$

The bunch of ions (see Fig. 8) formed at the leading edge of the trapezoidal modulation pulse makes one complete revolution along the drift orbit of radius ρ_2, catches up with the trailing edge of the next modulation pulse, becomes accelerated again and passes the analyzer exit slit S_3. Ions that in the first acceleration have got an energy gain ΔE_1, will acquire ΔE_2 in the second, and vice versa, ions 2 that in the first passing of modulator received an energy ΔE_2 will be next time accelerated by ΔE_1. Thus, after the first two accelerations the energy increment of all ions in the bunch (1–2) will be the same, $2\Delta E_0$; in other words, we have witnessed compensation of the scatter in energy acquired by the ions in two acceleration stages in the modulator. Significantly, the radial extent of the bunch will be mediated primarily by the width of the source slit S_0. A smooth variation of T or of the pulse repetition frequency within a certain small interval centered on the value defined by Eq. (9) brings about a variation of the net gain of energy and exit ion orbit radius while not compromising the compensation. The resultant ion beam shifts relative to the exit slit S_3 to form an ion current peak. This is how a mass spectrum is scanned in frequency.

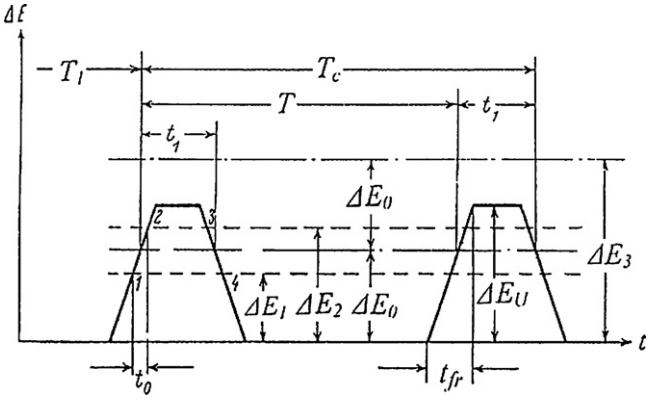

Fig. 8. Time correlations and operation modes of MRMS [16].

The dispersion of the instrument, or the change of the exit orbit diameter dD_3 ($D_3 = 2\rho_3$ in Fig. 7) corresponding to a change of the ion mass dM, can be derived in the following way [16]:

$$\frac{dE}{dT_C} = \frac{d\,\Delta E}{dT_C} = \frac{\Delta E_U}{t_{fr}}, \tag{10}$$

where ΔE is the increment of ion energy acquired in two accelerations in the modulator, E is the total energy of ions that can be written as $E = E_1S + \Delta E$, with E_1S being the energy of ions moving from the source along an orbit of radius ρ_1 (Fig. 7). According to Eq. (3):

$$\frac{M}{dM} = \frac{T_C}{dT_C}, \tag{11}$$

so that

$$\frac{dE\,M}{dM} = \frac{dE\,T_C}{dT_C} = \frac{T_C\,\Delta E_U}{t_{fr}}, \tag{12}$$

or

$$\frac{dE}{dM} = \frac{\Delta E_U T_C}{M t_{fr}}. \tag{13}$$

Now the dispersion equation can be recast in the form:

$$\frac{dD}{dM} = \frac{dD}{dE} \cdot \frac{dE}{dM}. \tag{14}$$

For rotation in a homogeneous magnetic field $E = kD^2$, whence $dE = 2kD$. Now

$$\frac{dD}{dM} = \frac{1}{M} \cdot \frac{\Delta E_U}{t_{fr}} \cdot \frac{T_C}{2kD}. \tag{15}$$

Express dispersion in terms of the diameters of the source and detector orbits (see Fig. 7), i.e., $D_1 = 2\rho_1$, $D_3 = 2\rho_3$, assuming $D = D_3$ and $\Delta E_U = \Delta E_3$. We obtain:

$$\Delta E_U \approx E_3 - E_1 = kD_3^2 - kD_1^2, \tag{16}$$

$$\frac{dD}{dM} = \frac{1}{M} \cdot \frac{k(D_3^2 - D_1^2)}{t_{fr}} \cdot \frac{T_C}{2kD_3}. \tag{17}$$

Finally we come to the following expression for the MRMS dispersion:

$$\frac{dD}{dM} = \frac{T_C}{t_{fr}} \cdot \frac{D_3 - D_1}{M} \cdot \frac{D_3 + D_1}{2D_1}. \tag{18}$$

If the analyzer exit slit S_3 is equal in width to the arriving ion bunch, i.e., $dD = S_3$, the MRMS resolving power at the half-maximum of the compensation peak will be:

$$R_{0.5\,\mathrm{h}} = \frac{2M}{\Delta M} = \frac{T_C}{t_{fr}} \cdot \frac{D_3 - D_1}{S_3} \cdot \frac{D_3 + D_1}{2D_1}. \tag{19}$$

This operation of the MRMS was called the compensation mode.

5.2. Resonance mode

Here $T = T_C$. In this case, the ions of bunch (1–2) which were first accelerated at the leading edge of the modulation curve, will make one complete turn in the drift orbit with radius ρ_2 (Fig. 7) and, on catching up again with the leading edge of the next pulse, will receive the second acceleration. The total energy increment will lie in the $2\Delta E_1 + 2\Delta E_2$ range; thus, the energy scatter will increase, with the result being that only a small part of ions with the energy $2\Delta E_0$ will arrive at the exit slit S_3. The resolving power of the instrument will now be substantially smaller than in the first case, where the ion scatter in energy was balanced out. This operation of the MRMS was called the resonance mode.

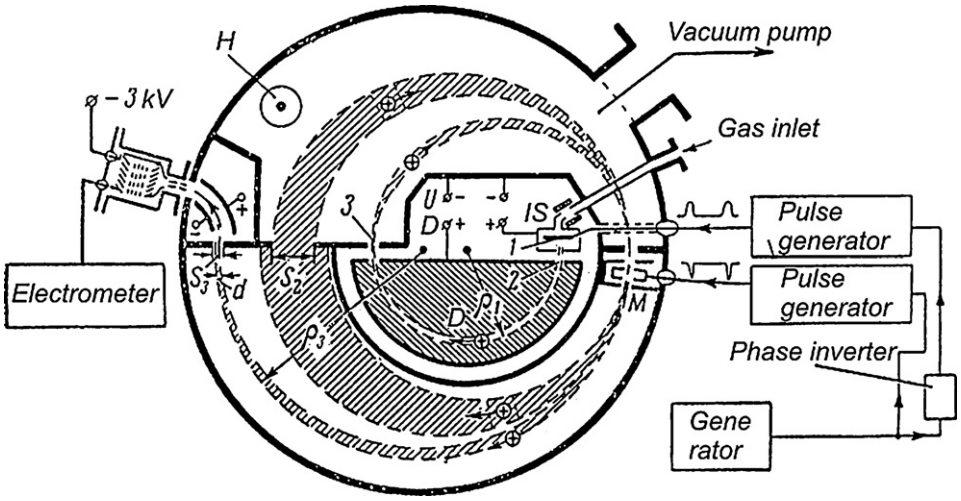

Fig. 9. Scheme of the mass analyzer with dee [17]: IS: ion source, 1: exit slit of ion source. 2: dee, 3: exit slit of dee, M: modulator, S_2: drift slit, and S_3: exit slit of analyzer.

5.3. Second compensation regime

$T = T_C + t_1$ (see Fig. 8). In this case, the ions of bunch (3–4) that were first accelerated at the trailing edge of the pulse will be driven by second acceleration to the leading edge of the next pulse, with the concomitant compensation of energy scatter as in case 1, i.e., $T = T_C - t_1$ for the (1 ± 2) ion bunch. This regime of operation was termed the upper compensation mode.

5.4. Spectrum of the same mass ions

Thus, the total spectrum of ions of the same mass, for a trapezoidal modulation curve, consists of three peaks corresponding to the three above cases: $T = T_C - t_1$, $T = T_C$, and $T = T_C + t_1$. Significantly, the position of the compensation peaks on the frequency axis is extremely sensitive to the amplitude of the modulator pulse, and that of the resonance peak depends on the pulse amplitude to a much lesser extent. As turned out later on, the theory developed in Ref. [16] was found to hold in the case where sinusoidal voltage is used for modulation, The compensation mode of MRMS operation found application in instruments with a high sensitivity and a resolving power of up to 20–30 thousand, which are currently employed in analytical works. The resonance mode is appropriate for instruments intended for measurement of fundamental physical constants, an area where high resolving power is at a premium. In this case the resolution needed is achieved with the aid of more narrow slits and a small part of ion beam is used only. The relation:

$$\omega_{ci} M_i = \text{const}, \tag{20}$$

which derives from Eq. (1) for ions of different masses performing cyclotron motion in the same magnetic field, is strictly met. Eq. (20) is similar to Eq. (5) which underpins Bleakney's theorem. While Eq. (5) underlies all measurements of ion or atomic masses with magnetic static arrangements, Eq. (20) is a basis for studying ion masses with cyclotron instruments, including the MRMS and RFMS.

6. MRMS with dee

The theory developed in Ref. [16] was used to build two magnetic resonance instruments at the same time. The first instrument employing two-stage separation of ions in time [17] operated in the compensation mode (Fig. 9). It used a pulsed source with ion accumulation during the pause between pulses. Ion bunches are accelerated in gap 2 to enter dee D, which represents essentially a closed nonmagnetic metallic box charged positively with respect to the analyzer walls. On exiting the dee, ions become additionally accelerated in gap 3, which permits them to turn round the source and enter the modulator. It was believed [17] that the dee would reduce the angular and energy scatter in the ion beam on the way from the source to modulator. This entailed, however, a radical change in the instrument design. The ion motion trajectory makes 2.5 turns, and the ion source and the modulator are mounted on the same side from the center of the analyzer. Also, the authors had to assume that it is the drift slit S_2 that acts as the exit slit of the first static stage of the mass spectrometer, rather than the modulator slit as is usually assumed in resonance instruments.

For a source orbit radius $\rho_1 = 50$ mm (see Fig. 9) and $\rho_3 = 70$ mm, the dispersion of this mass spectrometer per 1% of the mass change is, as follows from Eq. (18), ~50 mm. For the width of the exit slit $S_3 \approx 0.5$ mm, the resolving power of the instrument at half-maximum points of the mass line was as high as 10–11 thousand. As can be inferred from Eqs. (18) and (19), with the condition $T_C/t_{fr} = \text{const}$ met, the dispersion and resolving power of the MRMS does not depend on ion mass. This provides a possibility of mass measurement over a broad range without sacrificing accuracy. Ref. [17] presents spectra of doublets, from $M = 3$ u ($^1H^+{}_3$–$^1H^2D^+$) to $M = 36$ ($^1H^{35}Cl^+$–$^{36}Ar^+$). The fairly high resolving power of the instrument was complemented by a very good shape of the mass line, which evidences only a weak effect of the angular and energy scatter of ions in a beam. For an operating pressure in the analyzer of $\sim 3 \times 10^{-11}$ Torr and a fairly low ion beam energy, 400–700 eV, the mass line in a spectrum has practically no tails at the base. Table 1 lists the resolving power at different levels of the mass peak amplitude.

The maximum mass peak intensity ratio that can be measured (dynamic range of the mass-spectrometer) was as high as 10^6. The sensitivity of the instrument was limited primarily by the low energy of the ions and by the effect exerted on ion beam motion by stray electric fields at the inner surfaces and components of the analyzer.

The MRMS in question featuring a high resolving power and sensitivity was used to measure the mass spectrum of residual gases in the analyzer chamber [18]. The measurements were conducted in a vacuum of 10^{-7}–10^{-6} Torr. The sensitivity of the instrument

Table 1
The resolving power at different levels of mass peak amplitude.

$\% I_{max}$	50	10	1	0.1	0.01
$R_{0.5\,h}$	11,000	6200	3100	2200	1300

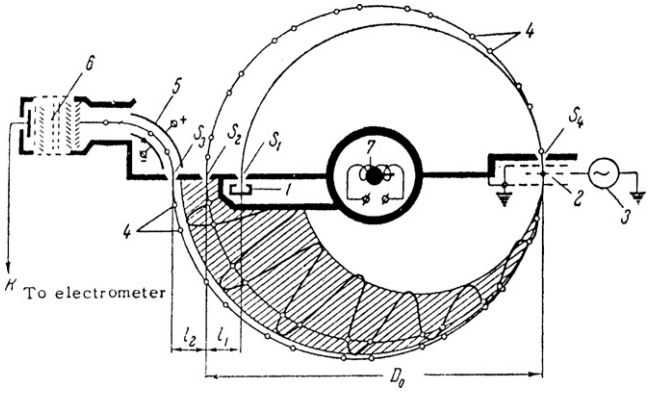

Fig. 10. Design schematic of the MRMS intended for measurement of the proton magnetic moment in nuclear magnetons [20]: 1: ion source; 2: modulator; 3: rf sinusoidal oscillator; 4: ion bunches; 5: extracting condenser; 6: secondary electron multiplier; 7: nuclear magnetic resonance probe. S_0: exit slit of ion source, S_1: modulator slits, S_2: drift slit, and S_3: exit slit of analyzer.

was high enough to permit reliable detection of the mass peaks corresponding to partial pressures of $\sim 5 \times 10^{-12}$ Torr. The measurements were performed in the 3–45 u mass range. Since the energy of the ionizing electrons could be as high as 140 eV, the spectrum evidenced the presence of doubly charged ions $^{14}N^{++}$, $^{16}O^{++}$. The high resolving power permitted reliable identification of all peaks in the mass spectrum, which related primarily to $^{1}H_2^{+}$, $^{12}C^{++}$, $^{14}N^{++}$, $^{16}O^{++}$, totally resolved triplet $^{12}C^{16}O^{+}$–N_2^{+}–$^{12}C_2H_4^{+}$, simple molecules, and organics. This instrument was used until recently to perform routine analyses required in studies of helium isotopes in solid and liquid geological samples. The instrument was modified in due time, and the modulator voltage was made sinusoidal.

6.1. MRMS with sinusoidal modulator voltage

The second MRMS which was built at Physico-Technical Institute in the early 1960s operated in the resonance mode and was intended for precision measurements of one of the most important electromagnetic physical constants, the magnetic moment of the proton in nuclear magnetons. It differed from the other MRMS designs developed at the PTI mainly in that its ion source operated in continuous mode, and the modulator voltage was sinusoidal, a feature that simplified considerably achieving the desired frequency, amplitude, and stability [19]. The instrument (see Fig. 10) operated on the 196th harmonic; said otherwise, the frequency of modulation was 196 times the cyclotron frequency of the ions to be studied. The magnetic field $H \approx 1300$ Oe was produced by a permanent magnet with pole pieces 350 mm in diameter, on which rings of soft iron with an outer diameter of 430 mm were put on to combat the influence of fringe fields on ion motion along the drift orbit between the first and second transits through the modulator. For a drift orbit diameter $D_0 = 224$ mm, $l_1 = 28$ mm, $l_2 = 26$ mm, and widths of the slits $S_0 = 0.2$ mm, $S_1 = 0.5$ mm, $S_2 = 0.6$ mm, and $S_3 = 0.4$ mm the instrument dispersion per 1% of mass change was ~400 mm, and the resolving power at half-maximum of a mass line $R_{0.5\,h} = (30–35) \times 10^3$. By analogy with Ref. [16], analytic expressions for the dispersion and resolving power with the ion beam modulated by sinusoidal voltage were obtained [19].

This analysis ended with a significant conclusion, namely, that the theory of modulation of an ion beam in a cyclotron instrument is strictly correct only for $\Delta\upsilon \ll \upsilon_0$, i.e., that the increment of velocity gained in the course of modulation should be significantly smaller than the velocity itself, the condition used by Bennett in a linear instrument [12]. In cases where this inequality fails in properly operating cyclotron instruments, the shape of the modulation curve is not strictly sinusoidal and is different in the first and second accelerations. The ion velocity after the second acceleration in the modulator being higher than that after the first one, l_2 should be smaller than l_1, so that in the resonance mode of operation the ion bunches from the leading and trailing parts of the sinusoid will enter simultaneously the exit slit of the MRMS. The movable slit S_2 (Fig. 10) enables to change l_1 and l_2 and so to optimize an exit mass peak.

7. Magnetic moment of proton in nuclear magneton units

By definition, the magnitude of the proton magnetic moment μ_p expressed in nuclear magnetons μ_0 is equal to the ratio of the spin precession frequency of the proton $f_n = (2\pi\mu_p/\pi h)H$ to its cyclotron frequency $f_{cp} = eH/2\pi M_p c$, measured in the same magnetic field (shielded proton magnetic moment, H_2O, sphere, 25 °C):

$$\frac{\mu_p'}{\mu_n} = \frac{f_n}{f_{cp}}, \tag{21}$$

where $\mu_n = eh/4\pi M_p c$ is the nuclear magneton, and h is the Planck constant. The frequency of the proton spin precession can be derived with a high precision from measurements of nuclear magnetic resonance, for instance, in a water sample. The major difficulty is encountered in determination of the proton cyclotron frequency. The problem can be simplified, however, because, as follows from Eq. (20), it is not necessary to measure the cyclotron frequency of the proton, actually; one can measure instead the cyclotron frequency of any other ion ω_{ci} and reduce it to ω_{cp} knowing precise values of the atom and the proton masses. Measurements of ω_{ci} were conducted on the $^{4}He^{+}$, $^{20}Ne^{++}$, and $^{20}Ne^{+}$ ions [20,21]. To include the effect of stray electric fields on the cyclotron frequencies, one resorted to linear extrapolation of ω_{ci} for two ions with masses M_1 and M_2 (for instance, $^{20}Ne^{+}$ and $^{4}He^{+}$) to zero mass. This procedure is essentially equivalent to measurement of the cyclotron frequency of an ion accelerated by an infinitely high accelerating voltage, compared with which the effect of stray electric fields (of a few Volts) may be safely neglected. This extrapolation may be considered correct subject to the condition that the stray electric fields remain constant over the whole trajectory of motion of ions of both types. It may be supposed that this condition was not met in the cited studies, with the result that extrapolation of ω_{ci} to zero mass could introduce errors in the final stage of μ_p/μ_n determination.

To take properly into account the magnetic field inhomogeneities over the MRMS drift orbit, the field was mapped at 12 or 24 points, and the correction to the cyclotron frequency calculated. Because within the modulator ions move with acceleration, this gives rise to a distortion of the cyclotron frequency being measured. The magnitude of this correction was calculated theoretically and introduced into the final result. The value thus obtained, $\mu_p/\mu_n = 2.79279 \pm 0.00002$ ($\pm 7.2 \times 10^{-6}$), differed noticeably from the value accepted officially by CODATA, but had a smaller uncertainty, which initiated a heated debate among scientists engaged in measurement of fundamental physical constants [22].

To exclude possible error in extrapolation of ω_{ci} to zero mass, a two-section ion source was designed producing simultaneously ions of two masses, more specifically, $^{4}He^{+}$–$^{20}Ne^{++}$, $^{4}He^{+}$–$^{20}Ne^{+}$, $^{4}He^{+}$–$^{40}Ar^{++}$, and $^{4}He^{+}$–$^{40}Ar^{+}$ [23,24]. In this case, the effect of stray electric fields on the cyclotron frequencies of ions in a pair would be substantially smaller than that experienced in Refs. [20,21]. In addition, the magnetic field inhomogeneity at the operating orbit was considerably reduced down to $\Delta B_z/B_0 \approx \pm 7 \times 10^{-6}$ (here B_0 is the magnetic field at the magnet gap center). In this study, we measured all the three magnetic field components at the operating orbit 224 mm in diameter, namely, the vertical ΔB_z, radial ΔB_ρ, and azimuthal ΔB_φ ones [25]. The resolving power at the half-maximum of the mass line was $\sim 5 \times 10^4$ throughout the mass

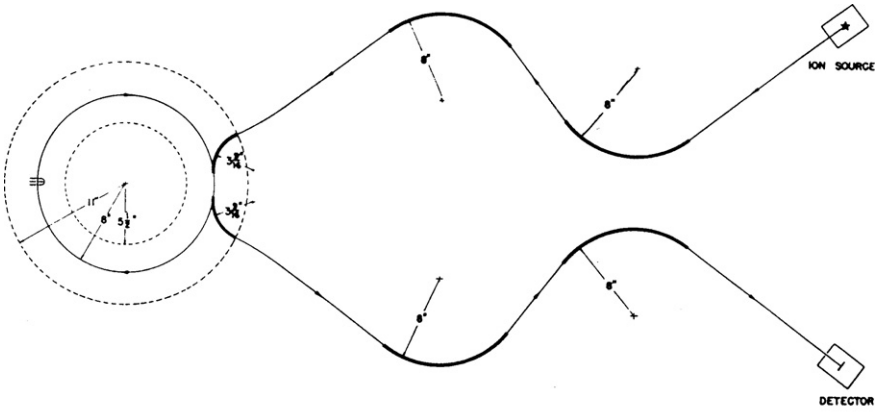

Fig. 11. Plan view of the complete ion orbit of RFMS [30].

range covered, 4–40. The instrument operated in the resonance mode [16], thus permitting one to calculate the modulator error, which originates from ions in the modulator moving with acceleration, so that the velocity increment is not exactly a sine function. We introduced also corrections accounting for the magnetic properties of the MRMS analyzer chamber and the magnetic effect of the cathode filament current in the ion source, and the relativistic correction, as well as estimated all possible errors that could be made in measurements and subsequent calculations. As the net result of this study, we came to the value $\mu_p/\mu_n = 2.7927744 \pm 0.0000012$ ($\pm 0.43 \times 10^{-6}$), which was entered without any changes into the 1973 Adjustment of the Fundamental Constants [26] and serves as a reference in determination of a number of electromagnetic physical constants until the publication of the next, 1986 Adjustment of the Fundamental Physical Constants [27]. This quantification of the μ_p/μ_n ratio was the most precise direct measurement of this value. In all later adjustments of fundamental physical constants (1998, 2002, 2006) the magnitude of the magnetic moment of the proton in nuclear magnetons is derived by calculation.

8. Radio frequency mass spectrometer

In 1967, L.G. Smith published the results of a study of the RFMS he had built at Princeton University [28]. In its principle of operation, this instrument resembles very much the MRMS. On the plan view in Fig. 11 is shown the complete ion orbit, and Fig. 12 presents the elevation view of the instrument. The major aspect that discriminates this RFMS from all magnetic resonance instruments is that the continuously operating ion source is placed well beyond the action of magnetic field. An ion beam is transported by two sequential toroidal lenses to the entrance of a cylindrical capacitor, which injects the beam into the magnetic field at the angle required to reach the RFMS operating orbit. The toroidal injector lenses not only focus the ion beam but feature a high dispersion in energy, i.e., they enhance the resolving power of the instrument. The ion beam makes two complete turns in the magnetic field and crosses twice the modulator located diametrically opposite to the entrance and exit slits of the instrument. The output ejector capacitor draws the ion beam out of the magnetic field and, acting in conjunction with two toroidal ejector lenses, which are identical to the injector ones, transports the beam to the entrance of the detector unit. Thus, the diagrams of injection of an ion beam into the RFMS mass analyzer and of its ejection out of it are absolutely symmetrical and are built of identical components.

The mass analyzer chamber is a cylinder ~560 mm in diameter and ~53 mm high. It was made of copper and was coated on the inside by gold to reduce or suppress the deleterious effect of contact potential differences and fringe electric fields on ion motion along the operating orbit. The modulator consists of three plane electrodes; the two outer ones are grounded, and to the third one, rf sinusoidal voltage is applied. In the modulator electrodes the entrance and exit slits are provided, together with the phase slit (Fig. 12). As already mentioned, the orbit of ion motion in an RFMS is a constant-radius spiral making two complete turns. This means that in two crossings of the modulator the ions should not get any velocity increment, with their velocity and radius remaining strictly constant. As shown in Ref. [28], this mode of operation can become realized only in the case where the frequency of the modulator voltage is related with the ion cyclotron frequency through the expression:

$$\omega = \left(\frac{n+1}{2}\right)\omega_c, \tag{22}$$

where n is an integer. From the very beginning of its design, the instrument was intended for measurement of the masses of light ions, and therefore, the goal was to obtain the largest possible resolving power. For this purpose toroidal lenses were chosen for injection and ejection of the ion beam out of magnetic field, the height of the entrance and exit analyzer slits was 6.35 mm, and the width of the slits was only 0.1 mm. It was found that, putting aside the losses in the mass analyzer, only 2–3% of the ion current leaving the source passed through the beam entrance and exit system [28]. The main losses of the current in the analyzer should be assigned to the vertical divergence of the ion beam in its motion along the trajectory ~2.55 m long, as well as to the extremely stringent resonance conditions; indeed, in two passages through the modulator the ions should not get any increment in velocity, otherwise they will not reach the detector and will not contribute to the output signal. It is thus clear that only a small part of the ion current leaving the source reaches the detector and contributes to the output signal. Hence, the RFMS sensitivity was fairly low, and the instrument could not be employed in analytical work.

9. Precise measurement of atomic masses

The RFMSs coped beautifully with the main goal for which they were designed in the first place, i.e., measurement of atomic masses. As seen from Eqs. (1) and (4), the strong magnetic field (up to 10^4 G) generated by the electromagnet and the extremely high ion energy (up to 25 keV) permit using very high frequencies (f = 500–2000 MHz) and harmonics of the cyclotron frequency ($n \leq 2500$). At the same time, the principle underlying RFMS operation, by which ions are not accelerated in the modulator and, therefore, there is no need in using high-frequency modulator voltage of a large amplitude, simplified considerably the work, as is

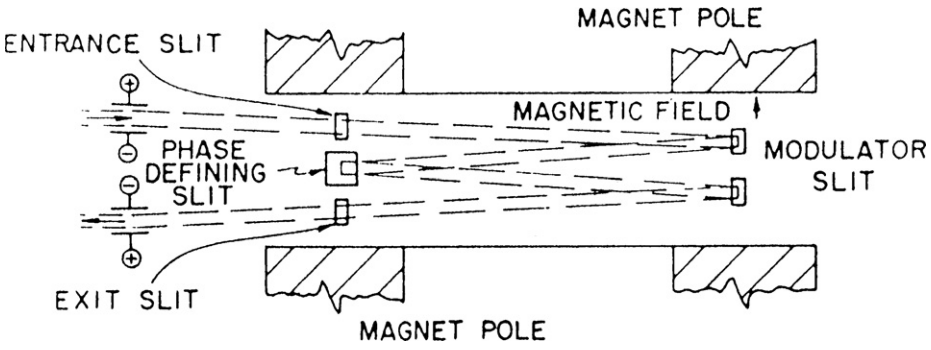

Fig. 12. Elevation view of the RFMS analyzer in the magnetic field [30].

seen from Eqs. (4), (6) and (7). Measurements were usually conducted at $R_{0.5\,h}$ = 250,000, and the maximum resolving power of the RFMS reached thus far is $\sim 4 \times 10^5$. Using the peak-matching method developed earlier [13] permitted one to determine the center of the mass peak with an accuracy of up to 1/2000–1/2500 of its FWHM (full width at half maximum); the resolving power obtained made it possible to measure atomic masses with a relative error of <1 ppb (10^{-9}).

This was demonstrated convincingly by L.G. Smith in his subsequent works. He measured the mass differences of 16 doublets containing atoms of 6 types: ^{1}H, ^{2}D, ^{14}N, ^{16}O, ^{35}Cl, and ^{37}Cl [29]. The measurements were conducted within the mass range extending from 16 u (CD_2–O) to 128 u (C_9H_{20}–$C_{10}H_8$). All the doublets consisted of two closely lying mass peaks, because for wide doublets with mass difference in excess of 1–2% of the measured mass and larger the effect of fringe electric fields on the motion of ions in RFMS could no longer be controlled, which entailed appearance of systematic errors in the atomic masses to be measured. Because the system of equations with unknown masses of atoms was overdefined, i.e., the number of equations it contained was much larger than that of unknowns, the results of measurements were treated by the least-squares method. The results were corrected for the kinetic energy of the molecules, the ionization potential, and the binding energy of molecules, which were either taken from reference books or calculated. The masses of the above six atoms were determined with a relative error ≤10 ppb, and their values were entered into the atomic mass tables and did not require refinement for decades.

In order to experimentally determine the masses of the hydrogen and helium isotopes from measurements of adequately wide doublets with a mass difference of ≥0.1% of the measured masses, an advanced version of the RFMS was developed [30]. The purpose was to reduce the effect of stray electric fields on the motion of different species of ions in the analyzer. The two pairs of vertically deflecting plates, with one at the entrance to the analyzer, and the other, at the exit from it, made it possible to control the entry and exit angles of beams in the analyzer and adjust the angles best suited for the two species of ions in the doublets. The second refinement consisted in properly positioning diaphragms between the ion source and the toroidal injector lenses, as well as in the modulator, which reduced the height of the ion beam. While all these changes reduced the sensitivity and the output current of the RFMS still more, they improved slightly the resolving power and, most important, suppressed to some extent the effect of fringe electric fields. The doublets measured were as follows: $^2D^+{}_2$–$^4He^+$, HT^+–$^4He^+$, $^2D^+{}_2$–HT^+, and HD^+–$^3He^+$, and the mass differences were determined to within a few thousandths of 1 ppm. As in the preceding work [29], the results of the measurements were corrected for the kinetic energy of the ions, chemical binding energy of atoms in the molecules, and the ionization potentials of the atoms and molecules. Seven series of measurements performed on the mass doublets of the hydrogen and helium isotopes with due allowance for the masses of protium and deuterium, whose values were taken from the same Ref. [29], completed with determination of the masses of the ^{3}He and ^{4}He isotopes, the mass of the tritium atom ^{3}T, and of the mass difference $\Delta M = M(^3\mathrm{T}) - M(^3\mathrm{He}) = (19968 \pm 7) \times 10^{-9}$ u, i.e., 18609 ± 7 eV. The values of atomic masses determined by L.G. Smith having substantially smaller uncertainties than practically all the known values of the masses, they were entered without any refinements in atomic mass tables [31].

The experimental data amassed by L.G. Smith served as a basis for one more publication [32] which contained recalculated or newly determined masses of the isotopes ^{1}H, ^{2}D, ^{3}T, ^{3}He, ^{4}He, ^{13}C, ^{14}C, ^{14}N, ^{15}N, ^{16}O and ^{19}F, as well as a refined mass difference between the tritium and helium-3 atoms. Indeed, β decay of the tritium nucleus produces the nucleus of helium-3, an electron, and an electron antineutrino, with liberation of an energy of ∼18.6 keV:

$$^3\mathrm{T} \rightarrow {}^3\mathrm{He}^+ + \mathrm{e}^- + \tilde{\nu} + 18.6\,\mathrm{keV} \qquad (23)$$

It thus follows that accurate knowledge of the mass difference between the tritium and helium-3 atoms, as well as the upper energy end point of the tritium β spectrum, could provide an estimate of the mass of the electron antineutrino $\tilde{\nu}$. While the magnitude of the mass difference $\Delta M = M(^3\mathrm{T}) - M(^3\mathrm{He})$ expressed in 10^{-9} u did not change after the publication of Ref. [29], it did change in energy units, because the adjustment of the fundamental physical constants carried out in 1973 [26] resulted in accepting a new coefficient to reduce the mass to energy units. The new value thus became $\Delta M = M(^3\mathrm{T}) - M(^3\mathrm{He}) = 18600.22$ eV, but this did not in any way clarify the problem of determination of the electron antineutrino mass.

10. Investigation of Smith's RFMS at Delft University

After the death of L.G. Smith in December 1972, the question arose of who and where would operate using RFMS. Neither at Princeton University nor in any other scientific center in the USA was there a person who was willing to put up himself/herself as a candidate to continue the work of L.G. Smith. And then a decision was reached to transfer the instrument to Delft University of Technology, the Netherlands [33]. Prior to disassembling the mass spectrometer in preparation for its transportation to Europe, it was thoroughly studied, its analytical characteristics were recorded, in particular, the mass spectrum of the well known doublet $^{14}N_2{}^+$–$^{12}C^{16}O^+$ was recorded as reference, and several sources of instability in operation identified, which could account for possible systematic errors from 0.3 to 1 ppb, for instance, in Ref. [31]. After the transportation in 1974, assembly and preliminary adjustment of the RFMS at Delft, the $^{14}N_2{}^+$–$^{12}C^{16}O^+$ doublet was recorded again, with the conclusion that the instrument did not suffer any damage in transportation, and one had only to adjust it

carefully and study its response. A conclusion was drawn [33,34] that the main problem was associated with unstable operation of the various systems and units of the instrument, which could bring about variation of the resolving power over a fairly broad range (from 10^5 to 4×10^5) on different days, or during one day even. It was found, for instance that the image of the exit slit of the ion source in the vicinity of the mass analyzer exit slit was diffuse and cross-shaped, thus reducing noticeably the $R_{0.5\,h}$. This could be initiated by fringe electric fields in the mass analyzer. To cut to the minimum the probability of generation of such fields, vacuum pumps and the actual conditions of evacuation were replaced and refined. One located also magnetic field inhomogeneities at a level of 15 μT and magnet vibrations that also contributed to these inhomogeneities and which depended on vibration frequency. A variety of factors were investigated that could produce instabilities in RFMS operation and account for possible systematic errors in Refs. [29,31]. Estimates of possible errors described in Refs. [33–35] amounted to a few times 10^{-9} u; it was believed that their inclusion into the results of atomic mass measurements and introduction of the corresponding corrections into the values of the atomic masses after so many years would most probably be wrong. All the more so that the RFMS analyzer has undergone substantial modifications. The conclusion that one should not introduce any corrections into the results published in Refs. [29,31] is attested by the following reasoning. The peak-matching method was experimentally shown to provide a possibility of locating the center of a mass-spectrum line with an error of 1/3500 rather than 1/2500, as stated in all publications of L.G. Smith. Thus, the newly revealed factors could both enhance and reduce the errors involved in the determination of atomic masses reported by L.G. Smith.

Regrettably, the immense amount of work performed at Delft University of Technology in 10 subsequent years [33–35] did not produce any new result of physical significance. Neither did the mass difference $\Delta M = M(^3\mathrm{T}) - M(^3\mathrm{He}) = 18573 \pm 7$ eV [36] derived from old results introduce a dominant note in arguments on the mass of the electron antineutrino. In 1983, studies with the instrument were stopped. The last publication devoted to the Smith's RFMS [37] overviewed the analytical performance of the instrument and presented a list of 9 problems of paramount importance that could have been solved with this instrument. Koets [37] believes that the resolving power of the RFMS at the peak half-maximum was 10^7 and even higher, and that the position of the peak center was determined with a standard deviation of $\sim 10^{-4}$ of mass peak width, so that the uncertainty of atomic mass measurements could be at a level of 10^{-11} or even less of the ion mass. Among possible problems that could be solved with the instrument were listed such as mass measurement of the doublet $^3\mathrm{T}^+ - ^3\mathrm{He}^+$ and evaluation of the mass of the electron antineutrino, measurement of the masses of other isomers, determination of the possible mass defect of the proton and antiproton, etc. The main purpose behind the publication of this paper [37], however, was a search for a new master of this unique instrument; significantly, the RFMS would be handed over free of charge, so that the only expenses one would have to pay for were the transportation costs. Prof. B. A. Mamyrin with colleagues, among them the author of this review, informed Delft University of their interest in acquiring the instrument, but our desires could not be realized because of financial limitations. The further fate of Smith's radio-frequency mass spectrometer is not known to the present author.

11. A new RFMS—MISTRAL intended for unique mass measurements

The analytical performance of the RFMS listed in Refs. [35,36] was extremely high ($R_{0.5\,h} = 10^7$), and it is possibly this factor that

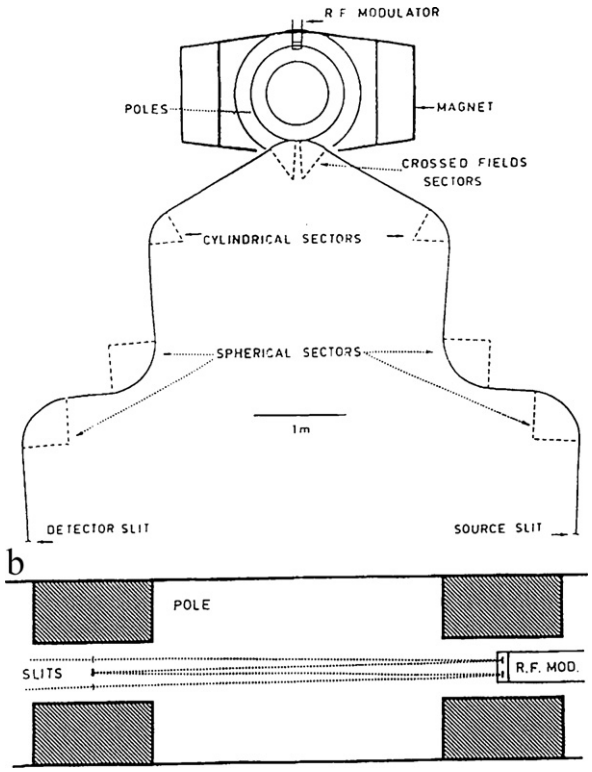

Fig. 13. (a) Schematic view of the whole France RFMS [38]. (b) Front view of the helicoidal ion orbit inside magnet.

turned out instrumental in the decision of French scientists to start building a mass spectrometer by the scheme of L.G. Smith with the goal to test the parity theorem (measurements of the proton and antiproton masses at CERN), make an estimate of the mass of the electron antineutrino $\tilde{\nu}$, and measure masses of exotic elements [38]. When it was built, it had a still more complex systems of ion beam injection into the mass analyzer, ejection of the beam out of the magnetic field zone, and its transportation to the detector (Fig. 13). As in the instrument designed by L.G. Smith, the beam injection and ejection systems were symmetrical, but now they contained a larger number of deflecting spherical and cylindrical capacitors. The beam entered the magnetic field zone not at right angles to it but very nearly along the tangent to it. Early in the design stage, the instrument was intended to provide a resolving power at FWHM of the mass line $\sim 10^6$. The relation defining the FWHM RFMS resolving power can be written as [39]:

$$R_{0.5\,h} = \frac{M}{\Delta M} = 2\pi n \left(\frac{D_m}{s}\right) \cdot \left(\frac{A_\delta}{\rho_o}\right), \tag{24}$$

where n is the number of the harmonic of the modulator voltage $\omega = (n + 1/2)\omega_c$, D_m is the amplitude of ion beam modulation, s specify the slit widths in the analyzer, with the exception of the phase-defining slit located in the central plane of the magnetic gap at midpoint between the entrance and exit analyzer slits (see Fig. 13).This slit enables to suppress background ion current and to detect resonance ions more accurately. A_δ is the dispersion in energy of the ion beam injection and ejection systems, ρ_0 is the radius of the ion orbit in magnetic field, $\rho_0 = (2UM/q)^{1/2}/B$. Introducing the actual instrument parameters ($n = 1500$, $D_m = 5$ mm, $s = 0.2$ mm, $A_\delta = 3000$ mm, $\rho_0 = 500$ mm), we come to $R_{0.5\,h} \sim 1.8 \times 10^6$ for the resolving power. The authors analyzed thoroughly the factors that could downgrade the resolving power. Among the most essential ones are the effect of magnetic field inhomogeneities on ion motion along the operating orbit, ion

modulation in the modulator gaps, and aberrations imparted on the way of the beam from the source to the detector which was estimated [39] as being capable to reduce $R_{0.5\,h}$ by ~30%.

A major unit in a radio-frequency mass spectrometer is the electromagnet generating a homogeneous field in the gap. For the chosen radius of ion motion in the analyzer $\rho_0 = 500$ mm, the inner diameter of the pole pieces was 660 mm, and the outer one, 1340 mm. The toroidal shape of the pole pieces was chosen probably to cut the mass of the pieces themselves and of the magnet as a whole. The height of the magnetic gap, i.e., the distance between the surfaces of the pole pieces, was 140 mm, and thus, the ratio of the difference between the diameters of the operating orbit and of the pole pieces (±340 mm) to the height of the magnetic gap was ~2.4, a figure of paramount importance from the standpoint of magnetic field homogeneity at the operating orbit and of the effect fringe magnetic fields at pole piece edges exert on this homogeneity. The total weight of the magnet is ~25 tons. The range of variation of the magnetic field induction lies in the range 0.1–0.8 T. In the early stage of the studies, the magnetic field homogeneity in the region of the operating orbit was fairly low, which did not permit one to reach resolving powers in excess of 3.0×10^5. It was maintained [39] that in order to obtain a resolving power of 10^6, the inhomogeneity of magnetic field at the ion orbit should not necessarily be at the level of 10^{-6}, because the ions are acted upon by an integrated field along all of the orbit. To be exact, the variation of the cyclotron period is driven by the difference between the real field B at the orbit and the ideal homogeneous field B_0. To calculate this variation $\Delta T_C/T_C$, one should know the magnitudes of all the magnetic field components B_Z, B_ρ, and B_φ along all of the ion orbit in the analyzer. By properly using magnetic shimming and a large number of plane coils through which computer-controlled electric current was passed (the coils are arranged at the inner planes of the pole pieces), one has managed to reduce the integral magnetic field inhomogeneity and obtain $R_{0.5\,h} = 10^6$ [40,41]. Therefore in all their later publications the authors, rather than estimating the magnetic field inhomogeneity at the ion orbit or at some of its points, just write that the inhomogeneity permitted obtaining a specified resolving power.

At the end of a careful adjustment and comprehensive studies, the radio-frequency mass spectrometer was installed at CERN, where it was immediately put to intense use. At the late 1990s, the radio-frequency mass spectrometer was assigned his present-day name MISTRAL. During the recent 15–20 years, it was actively used in tens of remarkable studies with considerable success, and it was subjected to permanent refinement and modifications dictated by the problem to be solved next. Practically in all these studies, in place of an ion source the on-line ISOLDE mass separator is employed, which is actually a facility dedicated to the production of a large variety of short-lived isotopes. Thus, the ion beam injection and ejection system of the RFMS ion beam exhibiting a fairly high energy dispersion was becoming replaced by the beam matching and transportation system from ISOLDE. This apparently accounts for the observation that the resolving power of MISTRAL specified in most of the recent publications does not exceed 10^5, while in earlier measurements $R_{0.5\,h}$ could reach 3×10^5 and even 10^6. As for the transmission and sensitivity, one can be referred to Ref. [41] which specifies that estimation of the mass analyzer transmission coefficient (with the ion beam injection and ejection system disconnected) yields ~1% for the width and height of the slits 0.4 and 10 mm, respectively, with the transmission of the mass spectrometer as a whole evaluated as 5×10^{-5}. This point has not been discussed thereafter, because the MISTRAL–ISOLDE combination operates with low enough input currents, and the output signal is detected by the single-ion counting technique.

12. High-precision mass spectrometric measurements at CERN

Analysis of all the studies of the French scientists reported on the issue being outside the scope of the present review, we shall dwell on a few of them only. To test the parity theorem, it is necessary to measure the masses of the proton and antiproton [41–43], but the comparison of these masses was not possible due to antiproton beam instabilities. There were reports of repeated measurements and refinements of the masses of the short-lived neutron-rich sodium isotopes $^{26-30}$Na [44,45] and the masses of the exotic magnesium isotopes $^{20-33}$Mg [45,46]. In one of the more recent studies [47] the French scientists applied the radio-frequency mass spectrometer MISTRAL to precision measurements of the mass of the short-lived radioactive isotope ^{11}Li ($T_{1/2} \sim 8$ ms), thus making it possible to determine the binding energy of excess neutrons in this exotic nucleus, a point of particular importance for the theory of strong interactions.

From the very beginning of its design in the 1980s, the rf mass spectrometer was intended to be a tool for solution of global-scale physical problems; indeed, after its building the instrument was never used in routine or standard mass measurements. After its installation at CERN in 1997, the instrument was assigned the name MISTRAL and was employed in precision mass measurements of only short-lived artificial isotopes produced with ISOLDE in bombardment of rather thick composite targets by high-energy proton beams. It is probably only the French scientists working on the MISTRAL radio-frequency mass spectrometer who remember that this instrument had been originally built by the scheme developed by L.G. Smith; incidentally, references to his studies ceased to appear already 10–15 years ago.

13. Analytical characteristics of the MRMS

As already mentioned, development of magnetic resonance mass spectrometers at the Physico-Technical Institute proceeded along two ways. Some MRMSs, having broad slits and featuring a high sensitivity, were used as analytic instruments to deal with various problems in the field of applications, and performed thousands of analyses of samples of natural and technogenic origin in the solid, liquid, and gaseous states. The refinements introduced into these instruments were aimed at increasing their absolute sensitivity, improving the stability of operation, and automation of measurements, and storage and treatment of the results obtained. In the other MRMSs intended for precision measurements of fundamental physical constants and atomic masses, primary emphasis was placed on development and refinement of new methods of calculation and of a theory which would be instrumental in calculating with a high accuracy ion motion in the instrument, identification and study of possible sources of errors, as well as on design of radically new systems and units for use in the mass spectrometer capable of eliminating or reducing to a minimum measurement errors in MRMSs intended for precision measurements of fundamental physical constants or atomic masses, a task that requires a different approach, more specifically, development of an accurate theory of ion motion. It appears pertinent to point out here an essential aspect of mass spectrometry, namely, that an increase of the resolving power by a factor 2–3 is a problem much more difficult to solve than increasing the sensitivity by the same factor of 2–3. At any rate, enhancing the resolving power, say, from $R_{0.5\,h} = 10^5$ to $R_{0.5\,h} = 3 \times 10^5$ is regarded as an achievement more significant than increasing the mass spectrometer sensitivity for partial pressure from 3×10^{-11} Torr to 10^{-11} Torr. Parallel development of the MRMSs of the above two types produced positive effects, because a successful solution of a problem reached in one

group was immediately introduced in the other instruments. To cite just one example, the method of magnetic field measurement in the ion orbit [48] by means of two nuclear magnetic resonance probes enjoyed immediately wide use. One of the probes, which is fixed, is used as reference and is located at the center of the magnetic gap, while the movable NMR probe runs along the operating orbit and can be positioned at one of 12 or 24 points on the circle. This technique permits one to map accurately the magnetic field and calculate the correction to the cyclotron period for a given ion species with a high precision. As another example, several MRMSs incorporate ion sources [49,50] whose ion optical systems incorporate crossed three-electrode lenses to focus the beams of the ions under study in two mutually perpendicular directions, an approach that made possible considerable enhancement of instrument sensitivity,

14. Investigation of helium isotopes with MRMS

It is well known that the ^{4}He isotope appears mostly as a product of the decay of transuranium elements, while ^{3}He forms both in fusion of deuterium and in β decay of tritium. For this reason, the helium isotope ratio ^{3}He/^{4}He can provide valuable information on processes occurring in the Nature, including those in the Earth's crust and mantle, on the Moon and the Sun, in the solar wind, in the mud and sulfides of black smokers, non-manganese nodules from the sea and ocean bottom, and in technogenic materials. The problems of helium isotopes investigations had for a long time been associated with the only MRMS available in the 1960–70s [17], which has been described above in details. In the course of operation, the instrument underwent continuously various refinements; indeed, the dee was removed and the mutual arrangement of all elements of the analyzer was optimized, next the high-frequency trapezoidal voltage supply of the modulator was replaced by a sinusoidal one, which simplified substantially the power supply unit of the mass spectrometer [51]. One introduced also new elements and systems which increased markedly the accuracy and reliability of measurements. In particular, a two-beam operational mode was adopted, in which ions of the two helium isotopes exiting simultaneously the source are recorded in different channels. As seen from Eq. (4), the radius of motion of ions with different masses in a magnetic field is proportional to $M^{1/2}$. Thus, the larger the ion mass, the larger is the radius. ^{3}He$^+$ ions move along their orbits of radius 47 mm, pass two times the modulator, and are detected at the MRMS exit. The resolving power of this channel is ∼5000 at half maximum of the mass line, which is high enough to permit resolving the ^{3}He$^+$ mass line from the H_3^+ and HD$^+$ lines. The second ^{4}He$^+$ detection channel is actually a static magnetic mass spectrometer with an ion motion radius of ∼55 mm. The ^{4}He$^+$ ion collector is placed at angular distance of 180° from the ion source (Fig. 14). Before the collector is an aperture slit, 1–2 mm wide, which is comparable in width to the source exit slit. Such wide slits were chosen to enhance the sensitivity with respect to ^{4}He$^+$. The resolving power of the static channel of ^{4}He$^+$ detection can be estimated as the ratio of the ion motion radius to the sum of the source and collector slit widths, with allowance for aberrations of various types. Rough estimation yields ∼10 for the resolving power, a figure large enough to provide complete separation of the two helium isotopes. The adjustment of the source in the two-beam operation mode is performed such that ion currents of both isotopes at the exit from the source are approximately equal in magnitude. One more essential refinement was introduced into the vacuum system of the instrument. A getter titanium pump cooled by liquid nitrogen was coupled to the analyzer chamber. This made it possible to reduce the residual pressure in the analyzer down to 10^{-8} Torr and support it in the static pumping regime, i.e., with the diffusion

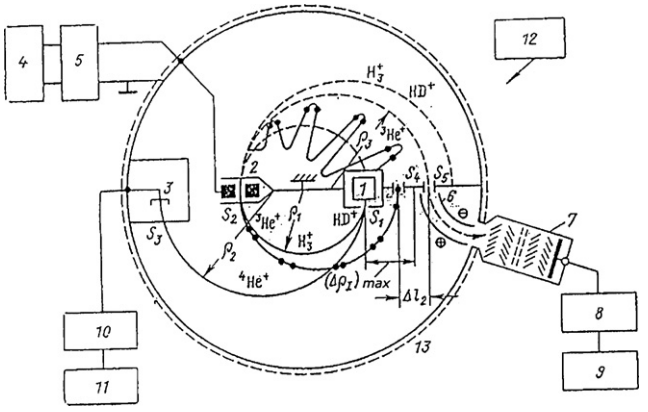

Fig. 14. Schematic view of the MRMS [52]: 1: ion source; 2: modulator; 3: ^{4}He$^+$ ion collector; 4: rf generator; 5: power amplifier; 6: extracting capacitor; 7: SEM; 8, 10: electrometric amplifiers; 9, 11: recording potentiometers; sample preparation and admission system; 13: magnetic field boundary. S_1: exit slit of ion source, S_2: modulator slits, S_3: slit of ^{4}He$^+$ collector, S_4: drift slit, S_5: exit slit of analyzer, ion bunches cut by drift slit S_4 from modulated sinusoidal ion beam are marked in bold points.

and backing pumps cut off for 10–15 min until the measurements are finished. It was reported [51,52] that the MRMS sensitivity was high enough to permit conducting reliable measurements of small amounts of ^{3}He, about 10^6 atoms, in the analyzer volume, and that it was determined primarily by the dark current of the secondary electron multiplier employed. The MRMS sensitivity to ^{4}He$^+$ is ∼10^9 atoms in a probe, and it is limited by the memory effect. The good shape of the mass-spectrum lines and the absence of tails in the H_3^+ and HD$^+$ peaks, as well as of ^{4}He$^+$ permitted measurements of the ^{3}He/^{4}He isotope ratio down to $\sim 5 \times 10^{-10}$. The instrument was calibrated using reference probes prepared with a particularly high accuracy.

This mass spectrometer was successfully used to perform hundreds of analyses of gas samples taken in gas and oil fields, from gases sampled in eruption of conventional and mud volcanoes, and mines. The ^{3}He/^{4}He isotope ratios found in these experiments ranged from 10^{-10} (in radioactive mineral beds) to >10^{-5} (in volcanic gases and over lithium-containing mineral beds) [53]. A major achievement reached with this instrument was the measurement of the ^{3}He/^{4}He isotope ratio in the Earth's atmosphere. By the time these measurements were started, the values of the ^{3}He/^{4}He ratio varied in the interval $(1.0–1.4) \times 10^{-6}$, with errors of 10–15%. The isotope composition of atmospheric helium was determined by comparing mass spectra of air sampled at different latitudes, longitudes (in different cities of the USSR), and heights (0–10,000 m) with those of reference mixtures prepared from pure ^{3}He and ^{4}He isotopes [54,55]. These measurements yielded the value ^{3}He/^{4}He = $(1.399 \pm 0.013) \times 10^{-6}$, which permitted a conclusion that the helium isotope ratio in air does not depend on geographic coordinates and altitude of sampling on the Earth, and, thus, should be considered as a specific geophysical constant.

15. Industrial magnetic resonance mass spectrometers for isotope investigation

The high analytical parameters of MRMS [51,52] and numerous demands to measure liquid, solid and gaseous samples led to the decision to build a limited series of four instruments with assistance of industry. In the course of building and adjustment, they were constantly improved, and, therefore, all these spectrometers differ slightly from one another, which required assigning them different names: MI-9301, MI-9302, MI-9303 (two instruments). Without delving into details, we shall highlight here the aspects in

which they departed from the prototype. These mass spectrometers were built around electromagnets powered by currents from 0.2 to 1 A. With the pole pieces 270 mm in diameter and a magnetic gap of ~40 mm, the magnetic induction can be varied from 0.08 to 0.8 T, allowing analysis of ions over a mass range of 2–170 u with the accelerating voltage is ~1600 V, and 4–340 u for an accelerating voltage of ~800 V [56]. The second essential feature that discriminated these instruments from their prototype was that all components of the vacuum system, including the mass analyzer chamber, were made of nonmagnetic stainless steel whose magnetic characteristics were specifically checked prior processing. In the course of machining and welding, however, as well as following a prolonged stay in a strong magnetic field, the stainless steel became itself magnetic. This brought about degradation of magnetic field uniformity along the ion motion orbit in the MRMS and deterioration of the resolving power. To exclude the magnetization effect, the analyzer chamber of the MI-9301 was manufactured of the VT-2 titanium alloy, which is known to be nonmagnetic. Application of the titanium alloy required carrying out a series of studies of the sorption property of this material and of the memory characteristics of the analyzer with respect to the helium and hydrogen isotopes [57]. The third significant difference was that the mass spectrometers were equipped by a two-channel system for admission of gases to be analyzed or to be used as reference. This system includes an ampoule breaker for consecutive opening in vacuum of ampoules with gases, scaled volumes for preparation of a sample for measurement, vessels for storage of pure isotopes of helium and hydrogen and of the reference gas mixtures with various $^3He/^4He$ isotope ratios. The inlet system is made of stainless steel and provided with independent high-vacuum pumping and high-temperature heating. Just as in the prototype mass spectrometer [51,52], in the new MI-9301, 02, 03 instruments a possibility is offered of operating in the mass-analyzer static pumping mode. When in this regime, the valve connecting the analyzer with the backing and diffusion pumps is closed after admission of the sample to be studied, leaving evacuation of chemically active gases desorbing from the walls and components of the analyzer to a titanium mirror cooled to the liquid nitrogen temperature [58].

These instruments having been developed primarily for analytical purposes, in particular, for helium isotope measurements, they provide two-beam (and even three-beam) operational modes, in which the $^3He^+$ and $^4He^+$ or $H_2{}^+$ ions exit simultaneously the source and move in a magnetic field along different orbits in accordance with Eq. (4). On making half-a-turn, $^4He^+$ ions strike the collector and are recorded. The resolving power of this static mass spectrometer is high enough to permit separation of the helium isotopes from the molecular protium $H_2{}^+$. $^3He^+$ ions move in an orbit ~67 mm in radius, enter after half a turn the modulator to get there an increment in velocity and radius, i.e., are analyzed by the magnetic resonance mass spectrometer. The schematic of the MI-9302 mass analyzer is presented in Fig. 15.

The analytical characteristics of all MI-9301, 02, 03 differing only little from one another, I am going to cite here only the most essential of them [56–58]. The maximum resolving power at half-maximum of the mass line $R_{0.5\,h} = 6 \times 10^4$. The sensitivity threshold to ^{40}Ar at $R_{0.5\,h} = 10^4$ is 2×10^5 atoms in the analyzer chamber volume, and to ^3He, $\sim 10^6$ atoms. The relative sensitivity to argon, as measured at the input to the secondary electron multiplier, is 5×10^{-5} A/Torr.

16. Applications of the helium method

Rather than listing here the numerous studies that were performed with the MRMS, including the MI-9301, 02, 03 series, we shall mention here only the recent publications reporting on isotope investigation of noble gases. Studies of the helium isotope ratio in mantle gases, in particular, those produced in volcanic eruptions on Kamchatka and Kuril islands [59], water of Iceland's geothermal sources [60], Baikal rift zone [61] etc. permit one to draw the conclusion that the high $^3He/^4He \geq 1 \times 10^{-5}$ ratio found there originates actually from the relic mantle helium which persists in the interior of the Earth from the time of its formation. Another important conclusion based on isotope measurements [62,63] was establishment of a global link between the $^3He/^4He$ ratio and the heat fluxes directed to the Earth's continental crust. Investigation of helium penetration into solids being strained in liquid helium (T = 0.6–4.2 K) revealed the existence of dislocation-assisted dynamic diffusion [64,65]. The amounts of this incorporated helium exceed by several orders of magnitude all known figures bearing on penetration of atoms into strained crystalline and amorphous materials.

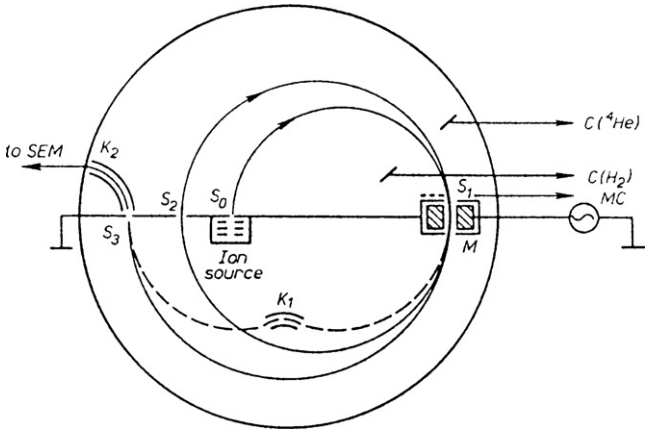

Fig. 15. Scheme of MRMS MI-9302 with ion collectors for $H_2{}^+$, $^4He^+$ and $^3He^+$ [56].

The high sensitivity of the MRMS and the techniques of isotope measurements of helium and other noble gases refined to perfection permitted their application to studies of the lunar soil brought back by the Luna-16 [66] and Luna-24 Moon-landing spacecraft. The weight of the regolith sample permitting complete analysis was $\sim 10^{-4}$ g. More recently, the helium isotope technique was employed to probe the solar wind transported to the Earth by cosmic dust [67]. Starting with mid-1980s, intense investigation of iron-manganese concretions raised from the bottom of the Pacific and Atlantic Oceans, as well as of the Finnish Gulf of the Baltic Sea was undertaken. These studies [68,69] were used to estimate the flux of the solar helium transported to the Earth by cosmic dust and yielded ~8 mm/10^3 y for the rate of growth of concretions. This figure exceeds by 2–3 orders of magnitude the values of concretion growth rate found by other, for instance, radiometric methods.

Convincing evidence for the impressive potential of the MRMS came from measurements of the residual spectrum in the analyzer chamber of the MI-9303 [70] conducted at pressures of 10^{-8}–10^{-10} Torr within the mass range of 1–140 u. The resolving power $R_{0.5\,h} = 1.5 \times 10^4$ of the instrument turned out high enough to separate practically all the mass multiplets, while the high sensitivity provided a possibility to study the variations of mass spectra at different pressures in the analyzer and different methods of its evacuation.

17. Determination of the tritium half-life

Another work that was made possible by the high sensitivity of the MRMS is the new helium-isotope method of measurement of the tritium half-life (see Eq. (23)). All methods of determination of this quantity that had been known at the time were based on abso-

lute measurements of the amounts of the tritium itself and of the ^{3}He forming in β decay, which entailed the need of high-precision measurements of volumes, partial pressures, and temperatures. The new method proposed for determination of $T_{1/2}$ of tritium [71] involves only relative measurements of the ^{3}He/^{4}He isotope ratios at times t_1 and t_2. The expressions for determination of $T_{1/2}$ can be derived in the following way. Suppose that we admitted at time t_0 into an ampoule a few cubic cm in volume of tritium $T_0^{(1)}$ and helium, the amounts not known in advance, and into the second identical ampoule, $T_0^{(2)}$ and $^4He^{(2)}$. The amounts of ^{3}He formed in β decay of tritium in the first ampoule by time t_1, and in the second ampoule, by time t_2, can be written as:

$$^3He^{(1)} = T_0^{(1)}\{1 - \exp[-\lambda(t_1 - t_0)]\} \quad (25)$$

$$^3He^{(2)} = T_0^{(2)}\{1 - \exp[-\lambda(t_2 - t_0)]\} \quad (26)$$

where the decay constant λ is related with the half-life through

$$\lambda = \frac{\ln 2}{T_{1/2}}. \quad (27)$$

If the ampoules are filled by a mixture of tritium and helium-4 from the same volume, and the partial pressures of each of the gases are equal, we come to:

$$\frac{T_0^{(1)}}{T_0^{(2)}} = \frac{^4He^{(1)}}{^4He^{(2)}} \quad (28)$$

Combining Eqs. (25)–(28), we obtain:

$$\frac{1 - \exp[-\ln 2(t_1 - t_0)/T_{1/2}]}{1 - \exp[-\ln 2(t_2 - t_0)/T_{1/2}]} = \frac{R_1}{R_2}, \quad (29)$$

where $R_1 = {}^3He^{(1)}/{}^4He^{(1)}$ and $R_2 = {}^3He^{(2)}/{}^4He^{(2)}$ are the isotope ratios measured in the first and second ampoules at times t_1 and t_2. Eq. (29) can now be used to derive $T_{1/2}$ of tritium.

This method was tested and used to advantage in practical work [72]. The duration of exposure of the gas sample, $t_2 - t_0$, was 846 days, the ampoules were stored at liquid nitrogen temperature, and measurements of the R_1 and R_2 isotope ratios in the probes were alternated with measurements on the reference samples. The authors studied and evaluated a number of possible sources which could contribute to the error in the final result. The value of the tritium half-life obtained in this study [72] is $T_{1/2} = (12.279 \pm 0.033)$ years. The helium isotope method was applied subsequently to measurements of the half-life of tritium in the atomic state, and to quantify the difference between the radioactive decay constants of tritium in its atomic and molecular states [73].

18. Ways to further upgrading of the MRMS sensitivity

Application of magnetic resonance mass spectrometers possessing a high sensitivity to various problems of applied and fundamental nature was constantly accompanied by their refinements and a further improvement of analytical performance. One of the ways to upgrading the reliability of measurements of the isotopes of helium and other noble gases in solid and liquid samples lies in ensuring as complete as possible extraction of these gases from metals, minerals, crystals, and water. The principle of operation of vacuum extraction systems intended for solid samples is based on heating of the samples in a corundum crucible by a programmable, computer-controlled system which would permit one to raise the temperature linearly with time with different rates up to ~1300 °C [74,75]. To purify inert gases of chemically active gaseous impurities, one usually resorts to traps with activated carbon which are cooled by liquid nitrogen, $T = -196$ °C, and titanium getter at $T \sim 400$ °C. Extraction of inert gases from liquid samples is made frequently difficult by the need to know the absolute amounts of the dissolved gases, and therefore the volumes of the extraction system should be measured with as high an accuracy as possible [76].

Another way of improving the reliability and accuracy of helium-isotope measurements involves direct enhancement of the MRMS sensitivity. As already mentioned, when operated in the static pumping mode and widths of the slits in the ion source, modulator, and detector of ~1 mm or more, the absolute sensitivity of the instruments [51,52,56,58] was found to be $\sim 10^6$ atoms of ^{3}He for an analyzer chamber volume of $(1.5–2) \times 10^{-3}$ m^3. A careful analysis of the operation of the instruments suggested that the main factors imposing restriction on the absolute and isotopic sensitivity of the MRMS are dark currents of secondary electron multipliers (SEM-1, SEM-2, SEM-6), memory effects with respect to the helium isotopes, the presence in the analyzers of hydrogen isotopes, and an increase of the background due to tails of the HD^+ and H_3^+ peaks and of the $^3T^+$ peak at the location of the $^3He^+$ peak [77]. Incidentally, in all the available MRMSs evacuation is provided by backing oil and diffusion pumps, so that the large number of mass lines belonging to organic molecules observed in the residual gas spectrum [70] should be apparently assigned to this feature of the instrument. To reduce the background due to the secondary electron multiplier, one started to cool it with liquid nitrogen. It was found possible to reduce the ^{3}He memory effect by prolonged heating and "washing" of the analyzer with helium-4 at a pressure of 10^{-6} Torr. The dominant contribution to the increase of sensitivity was made by transferring operation of the detection system to single-ion counting mode. The net result of all these improvements was reducing the minimum amount of ^{3}He in the mass analyzer volume that can be measured with an error of ~50% to 3×10^4 atoms, with the counting time of the signal and background pulses being ≥10 min. Estimates [77] suggest that the minimum measurable ^{3}He/^{4}He ratio decreased to 2×10^{-11}, and that the isotope ratio at a level of 10^{-10} could now be determined to within ~20%. Incidentally, transition to oil-free pumping could possibly bring further progress in the enhancement of the MRMS sensitivity.

While in monograph [78] one can find some details in the design and operation of the MRMSs which feature a high sensitivity and are employed in analytical work bearing on geology, geochronology, and geochemistry, it does not, however, approach the aspects associated with the specifics of design of instruments possessing a high resolving power. The PTI has reached some interesting and promising results in this area of instrument design for science and technology as well.

19. MRMS with a high resolving power and development of an adequate accurate theory

As already pointed out, the equation for tritium nucleus decay (23) contains the mass of the electron antineutrino $\tilde{\nu}$, whose determination requires the knowledge of the mass difference of the doublet $^3T^+$–$^3He^+$ and the high-energy end point of the tritium β spectrum. Knowledge of these quantities would permit one to estimate the $\tilde{\nu}$ mass, provided it is nonzero. In the 1970s, for the specific purpose of measuring the tritium decay constants one designed extremely complicated equipment (electron spectrometers) and used ion-cyclotron resonance Fourier-transform spectrometers with superconducting magnets, the last word in instrument design at the time. Very stringent requirements were imposed on these measurements, making them extremely difficult to perform. First, the mass difference $^3T^+$–$^3He^+ \approx 0.00002$ u, and hence, the resolving power of mass spectrometer at the base of mass line should be $R = M/\Delta M = 3/0.00002 = 1.5 \times 10^5$. Second, because the mass of the electron antineutrino is so small as to be close to zero (assume it to be ~1 eV), and 1 u ≈ 930 MeV, the relative error of mass difference determination should be at a level of

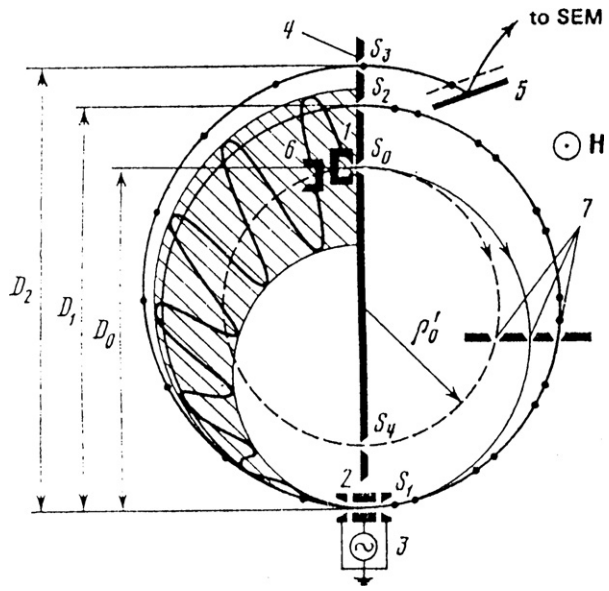

Fig. 16. Schematic representation of the MRMS analyzer: 1: ion source; 2: modulator;. 3: rf generator; 4: ion packets; 5: reflecting gap; 6: 360° collector; 7: aperture slits [79].

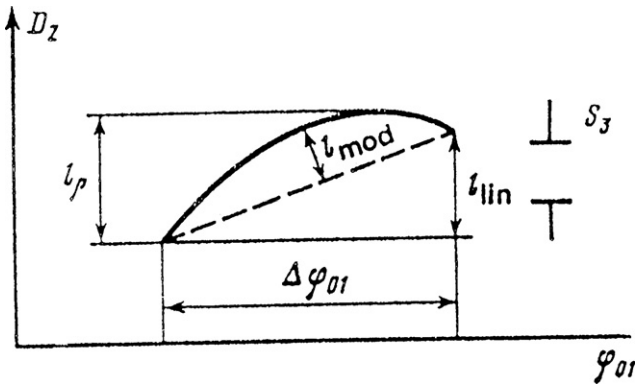

Fig. 17. Theoretical shape of an ion bunch [79].

10^{-9} u. Third, tritium is a radioactive material, and its admission to the mass analyzer would entail an increase of the dark current of secondary electron multipliers by several orders of magnitude, thus precluding precise measurement of masses or mass differences.

Development of MRMSs with a resolving power $R = 1.5 \times 10^5$ at peak base started with formulation of a theory describing the motion of ions in the instrument (Fig. 16) operated in the compensation mode. The equations of ion motion in the analyzer were similar to those used to calculate the modulation correction in measurements of the proton magnetic moment in nuclear magnetons [23,24], the only difference being that the instrument operated at that time in the resonance mode, and that it made use of a two-gap grid modulator. To increase the transmission coefficient, ensure preservation of the ion current on its way from the source to detector, and to reach the maximum possible sensitivity of the MRMS while retaining a high resolving power, we used a three-gap grid-free modulator. The slit in the fairly thick central electrode to which high-frequency modulator voltage is applied was considered in a first approximation as a field-free space traversed by ions which were accelerated in the first gap. With this point in mind, the motion of ions in the MRMS mass analyzer, from the source to detector, can be divided in 9 parts and described by nine transcendental equations relating the phases and transit angles of ions crossing the electrode gaps of the three-chamber modulator in the first and second transits. The first equation describes ion motion from the source exit slit S_0 to the modulator slit S_1, six equations describe motion in the three modulator gaps in the first and second transits, one equation relates to ion motion in the drift orbit between the first and second modulator transits, and the last equation describes the ion motion from the modulator to the exit slit S_3. The geometric, electrical, and frequency parameters of the analyzer enter these equations as coefficients. Setting the phase φ_{01} at the first injection of ions into modulator and solving the coupled equations thus obtained, we find the increment to the ion orbit diameter after two transits by the ions of the modulator. The computer-calculated arrangement of the bunch of ions before the exit slit S_3 is shown in Fig. 17. The shape of the bunch, its size, and position relative to the exit slit S_3 are determined by the width of the drift slit S_2, modulator parameters, and the nonlinear dependence of the orbit radius increment of ions on their injection phase in the first and second accelerations in the modulator. The compensation regime becomes realized when the ion bunch is oriented with respect to S_3 such that $l_{lin} = 0$. In this case, the ion bunch has a minimum dimension in the radial direction, l_{mod}, thus ensuring the maximum sensitivity of the analyzer.

The relation obtained for the resolving power at the mass line base can be written as:

$$R = \frac{M}{\Delta M} = \left(\frac{2\pi n}{\sum}\right)\left(\frac{dD_2}{dq}\right), \tag{30}$$

where n is the number of the modulator voltage harmonic, $q = 2\pi(f/f_c - n)$, and Σ is the sum of the widths of the ion bunch image at the analyzer exit slit and of the slit S_3 itself:

$$\sum = S_0 + \left(\frac{D_0}{2}\right)\frac{1 - D_0}{D_2}\left(\gamma^2 + \frac{\Delta U_0}{U_0}\right) + l_{mag} + l_{\mathrm{mod}} + S_3. \tag{31}$$

Here D_0 and D_2 are the orbit diameters (Fig. 16), γ is one half of the beam divergence angle at the ion source exit, ΔU_0 is the width of the ion distribution in energy at the source exit, U_0 is the potential difference accelerating ions in the source, I_{mag} is the ion beam broadening originating from magnetic field inhomogeneities, and I_{mod} is the beam broadening caused by the modulation processes. We derived also an expression for the MRMS sensitivity:

$$\eta = (k - l_{\mathrm{mod}})\frac{(2r_k l_{\mathrm{mod}} - l_{\mathrm{mod}}^2)^{1/2}}{\pi D_0}, \tag{32}$$

where r_k is the ion beam curvature radius, and k is found from Eq. (31): $k = S_0 + I_{mod}$. The quantity η has the dimension of length and specifies the part of the source exit slit S_0 from which the output current reaches the exit analyzer slit S_3. A search for the extremum of Eq. (32) showed that η reaches maximum when

$$S_0 = 2l_{\mathrm{mod}}. \tag{33}$$

Thus using Eqs. (31) and (33) one can derive from the condition of maximum sensitivity for a given resolving power the conditions specifying selection of the widths of slits S_0 and S_2. To find the optimum parameters of the MRMS analyzer, a special computer program was developed. This program included the equations of ion motion in the analyzer and Eqs. (30)–(33). The parameters obtained for the given values $R = M/\Delta M = 1.5 \times 10^5$, $B = 0.12$ T, $n = 100$ were as follows $D_0 = 186$ mm, $D_1 = 214$ mm, $D_2 = 232$ mm, $U_{mod}/U_0 = 0.27$, $\Sigma = 109$ μm, $S_0 = 27$ μm, $S_2 = 1.2$ mm, $S_3 = 55$ μm, and $\eta = 0.23$ μm. The widths of the first and second accelerating gaps are $d_1 = 1$ mm, $d_3 = 1$ mm, and the width of field-free drift chamber, i.e., the thickness of the central electrode in the modulator $d_2 = 2.4$ mm. For these parameters, the calculated instrument dispersion is 160 mm per 1% of ion mass change.

The data obtained in these calculations were employed to design an MRMS incorporating a permanent magnet, vacuum chamber

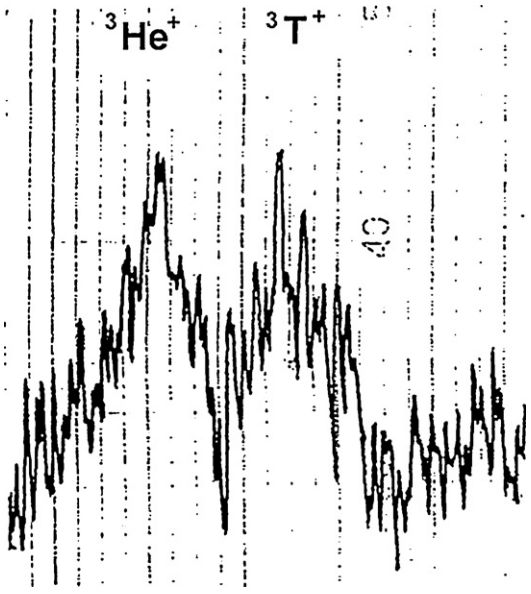

Fig. 18. Mass spectrum of the $^3He^+$–$^3T^+$ doublet [79].

and the high-frequency generator from the instrument used earlier to measure the proton magnetic moment in nuclear magnetons [23,24]. The instrument was adjusted to provide the maximum resolving power by translating within narrow limits the drift slit S_2 and turning the exit slit S_3 relative to magnetic lines of force, as well as by adjusting properly to an optimum level the frequencies, all supply voltages, and currents. After a careful adjustment of all parameters and setting $n = 110$, the resolving power of the instrument at half-maximum of the $^3He^+$ mass line was as high as $R_{0.5\,h} = 350{,}000$. The peak had a proper "good" shape, a signature of all MRMSs. The relative sensitivity of the static stage (radius ρ_0, exit slit S_4) was 2.5×10^{-4} A/Torr, and the sensitivity in the dynamic mode at maximum resolving power, $\sim 7.5 \times 10^{-8}$ A/Torr. The results of the calculations were corroborated by experiments. For proper visualization of the resolving power of the instrument, we recorded a series of spectra of the doublet $^3T^+$–$^3He^+$ (Fig. 18). The spectrum is seen to be pervaded by pulses of the SEM dark current originating from β decay of tritium nuclei on the surface of multiplier dynodes and surrounding components in the detector system of the MRMS. The constant component of the dark current exceeded by 2-3 orders of magnitude the amplitudes of the peaks in the doublet. Despite the background current of the β electrons, the $^3T^+$ and $^3He^+$ peaks are separated well enough, thus permitting us to estimate the mass difference $\Delta M = M(^3T) - M(^3He) \approx 18600$ eV, but the error of determination was so large (≥200 eV) that this result was never published.

To reduce the dark current due to the tritium β electrons, an ion beam detector was developed [80] that was based on transformation of ions into secondary electrons which are accelerated to an energy of ~30 keV, i.e., higher than the maximum β electron energy (~18.6 keV), and strike the scintillator. The scintillator is coated by a layer of photoresist of a specified thickness, which, while stopping the β electrons, lets the accelerated electrons pass, to be recorded subsequently in the single counting mode. This detector reduced considerably the background, but this MRMS was never employed thereafter in doublet mass measurements.

19.1. Second method of MRMS calculation

To further improve the analytical performance of the MRMS and to study the influence of various parameters on these characteristics, a novel method describing ion motion in the mass analyzer was developed [81]. In contrast to the approach employed in Ref. [79], this method took into account the distribution of ions at their exit from the source in energy, exit angle, and coordinate within the width of the exit slit S_0 (Fig. 16), and the effect crossed magnetic and electric fields exert on ion motion in modulator gaps of specified geometric dimensions. The ion motion equations were derived under the assumption that the origin of coordinates lies at the center of S_0. We assumed the trajectory of ion motion in the analyzer to be made up of 10 stages (in Ref. [79] there were 9 of them). The transit over the drift orbit after the first passage of the modulator was split into two parts, namely, one before the drift slit S_2 and the other, after it, up to the second entry into the modulator. Each stage of motion was identified with a system of from 4 to 6 equations describing variation of the ion trajectory radius, the coordinate along the y axis on which all analyzer slits are located, ion velocities, phases of the modulator voltage at which an ion enters the corresponding modulator gaps, and the angles at which an ion enters the modulator gaps.

To solve this system made up of about 50 equations, a program was developed which permitted one to model the MRMS operation in different modes. Modeling of the analyzer starts with setting the magnetic field B, the amplitude of the high-frequency modulator voltage U, the charge and mass of the ion m/q, and geometric parameters, more specifically, the distances from the center of the source exit slit S_0 to the center of the modulator slit S_1, and between the slits S_0 and S_3, and the widths of the slits S_0–S_3 and of the gaps in the modulator, d_1–d_2–d_3. The operation of the program was tested by calculating the modulator correction used in determination of μ_p/μ_n [23,24].The new value of this correction, $\Delta_{mod} = -0.000013648$, differs from the old one by 1×10^{-8}. The program made it possible to estimate the influence of individual parameters on the analytical performance of the instrument in cases where experimental studies are impossible or prohibitively difficult to conduct. Such parameters are the energy scatter of ions at the exit from the source, the amplitude and phase instabilities of the modulator voltage, variation of its harmonic composition, etc. A result of utmost importance was estimation of allowable energy scatter of ions in a beam. For scatters of 0.1–0.2 eV, the resolving power becomes as high as $R_{0.5\,h} \sim 350{,}000$, and for scatter of ~1 eV, $R_{0.5\,h}$ falls by 10%. The experiments provided convincing evidence for the validity of the above calculations.

19.2. Third method of MRMS calculation

Breaking up the trajectory of ion motion in the MRMS into 10 parts [81] was used in calculation of the instrument with a resolving power $R_{0.5\,h} \sim 10^6$. Another approach employed for this purpose is described in Ref. [82]. In each section of their motion, ions are assumed to be acted upon either only by a constant magnetic field or by a superposition of a constant magnetic field and an ac electric field. The starting parameters are the ion coordinates at the exit slit of the ion source, ion energy, angle of exit from the source, and frequency and phase of the high-frequency modulator voltage. In the study being described here, the cyclotron frequency harmonic number was chosen to be $\omega/\omega_c = 200$. One also sets the magnetic field B_0, amplitude of the modulator voltage U, ion mass and charge m/q, and all geometric dimensions of the analyzer specified above in the consideration of Ref. [81]. Equations of ion motion were composed for all 10 sections, the final conditions of ion flight in the first section becoming the starting conditions for the second section, and so on. The corresponding computer program was written in FoxPro and C. The part of the program dealing with calculations presents the results in the numerical and graphical forms. The other part of the program serves actually as an interface for input of the analyzer parameters and semiautomatic adjustment of the parameters of the instrument being modeled; it can be used for acquisition of

the results of calculations and their transfer to the database for subsequent additional treatment.

The operational regime of the MRMS is reached by introducing certain additional links between the set mass analyzer parameters (for instance, in the compensation regime all ions in a bunch should acquire in two transits of the modulator the same velocity increment) [16]. It is finding the set of the parameters at which a mass peak is observed that can be identified with adjustment of a real instrument. The programmed regime of adjustment is based essentially on calculation of the central trajectory of ions and estimation of the first-order aberrations, which permits one to obtain the resolving power $R_{0.5\,h}$, the efficiency of use of the current K_1, and direct transit voltage at which an ion after the first passage through the modulator achieves the exit slit S_3, as well as to estimate the precision of adjustment. Testing the program revealed that increasing the number of steps involved in setting of the parameters from 2 to 10 entails a considerable increase of the time of computation, while the associated changes in the resolving power and other characteristics are virtually negligible. The program permitted us to investigate the operation of the first static stage of the instrument, direct ejection mode, and the resonance and compensation MRMS modes. We also studied thoroughly the dependence of $R_{0.5\,h}$ and K_1 on the amplitude of modulator voltage for different values of diameters D_0 and D_2, as well as on the difference between the diameters $(D_2 - D_0)$, widths of the slits S_0, S_2, S_3, widths of accelerating gaps d_1 and d_3, as well as on the width of the field-free space d_2 for both the symmetric and asymmetric modulator, etc. These calculations combined with analysis of the data thus obtained yielded the optimum parameters of the analyzer with which the MRMS resolving power becomes as large as $R_{0.5\,h} \approx 1.35 \times 10^6$ for the efficiency of use of the current $K_1 \approx 0.006$. The calculations showed also the MRMS system to be stable against the variation of the geometric, electrical, and frequency parameters over a broad range. A comparison of the results of calculations amassed in this study with experimental data reported in Ref. [79] and calculations described in Ref. [81] suggests that a noticeable increase of the diameter of ion motion in the static stage of the mass spectrometer D_0 from 186 mm to 350 mm, with the slit widths in the source and modulator left practically unchanged, would increase the resolving power of the first stage nearly twofold. Transition of the harmonic number from $n = 110$ [79] to the calculated harmonic with $n = 200$ should likewise bring about growth of $R_{0.5\,h}$ by nearly a factor 2. All this provided reasonable grounds to believe that an MRMS with a resolving power $R_{0.5\,h} \sim 10^6$ can be built.

20. MRMS with a resolving power of ~10^6

The above calculations provided a sound basis for starting in the late 1990s design of an MRMS with a calculated resolving power at half-height of the mass line of $\sim 10^6$ and a mass range covered 3–200 u. The basic component of the instrument is an electromagnet [83] with the induction variable in the 0.05–0.5 T. The diameter of the pole pieces of the magnet is ~600 mm, and they are spaced about ~53 mm apart. The specific design of the magnet and in particular the fastening of magnetic poles and pole tips to yoke make it possible to adjust the homogeneity of magnetic induction at the circular dia.-400 mm operating orbit of the MRMS with a high enough precision and reproducibility. The inhomogeneity of the vertical component of magnetic induction measured at 24 points of the orbit with two nuclear magnetic resonance sensors, one of them movable and the other fixed at the center of the magnetic gap [48], is $\Delta B_z/B_0 \leq \pm 1 \times 10^{-5}$. The magnetic field instability over an interval of a few minutes is less than 10^{-6} of B_0 at magnetic gap center. The vacuum chamber of the MRMS analyzer is made of a nonmagnetic titanium alloy. The main difficulties were encountered in designing and manufacture of a high-frequency generator with the frequency variable within (7.5–52) MHz and an output voltage of (400–600) V. Extremely high requirements are imposed on the output characteristics of this generator; indeed, the output voltage should be strictly sinusoidal, the level of the higher harmonics multiples of the main frequency should not exceed $\sim 10^{-3}$ of the level of the main signal, the frequency stability should be $\Delta f/f \sim 10^{-7}$ or better over tens of seconds, and the amplitude stability of the output sinusoidal voltage should be $\Delta U/U \sim 10^{-4}$. Obviously enough, the frequency range had to be split into several parts. The system represents actually a powerful multi-stage arrangement whose output stages operate in the amplification-doubling mode. For the master oscillator one can use only a conventional RC generator, because the various frequency synthesizers and generators whose operation is based on frequency mixing cannot be integrated into the compensation regime of MRMS operation. It was found that the requirements imposed by us on the output characteristics of a high-frequency oscillator are so alien to engineers engaged in development of such equipment that the staggering price they asked forced us to start building of the generator on our own. This work will consume very much time and will delay the start-up of the instrument for an indefinite time.

21. Conclusion

We have considered the design, analytical performance, and the area of applications of mass spectrometers whose principle of operation depends essentially on the cyclotron frequencies of ions moving in a magnetic field depending only on their mass to charge ratio and the strength of the magnetic field. Because the product of the cyclotron frequency of ions by their mass in the same field is a constant, and frequency measurements are among the most accurate of all kinds of measurements, the RFMS and MRMS cyclotron instruments offer one a possibility to measure masses with a very high precision. This is favored by the high resolving power that can reach hundreds of thousands at half-maximum of a mass peak. It was shown that the resolving power of these instruments does not depend on the mass of the ion to be measured and is essentially the same over a wide mass range. In contrast to the RFMS, the MRMS can operate in two regimes, resonance and compensation; significantly, while the latter features high resolving power and sensitivity at the same time, in the compensation mode the amplitude of the output signal depends on that of the modulator voltage, a factor to be taken into account when operating with wide doublets. The high performance of the MRMS permits using these instruments in analysis of the various natural and technogenic samples. Novel applications of the MRMS may be connected with a study of the noble gases isotopes (from helium to xenon) for solution of important problems in geology, geochronology, cosmic chemistry, oceanography, etc. Moreover there are some special interesting tasks concerned with helium isotope ratio changes in the construction materials used in Tokamacs operating with the deuterium or deuterium-tritium plasma, in samples of Antarctic ice and the ice of ultradeep drill hole at the Vostok station, etc.

References

[1] W. Bleakney, J.A. Hipple Jr., Phys. Rev. 53 (1938) 521–529.
[2] V.B. Fiks, New mass spectrometry method, in: Proceedings of the scientific-technical conference, Polytechnic Institute, Leningrad, USSR, 1949, p. 25 (in Russian).
[3] S.A. Goudsmit, Phys. Rev. 74 (5) (1948) 622–623.
[4] L.G. Smith, Rev. Sci. Instrum. 22 (2) (1951) 115–116.
[5] E.E. Hays, P.I. Richards, S.A. Goudsmit, Phys. Rev. 84 (4) (1951) 824.
[6] N.I. Ionov, B.A. Mamyrin, V.B. Fiks, Resonance magnetic mass spectrometer with high resolving power, Zh. Tekh. Fiz. 23 (11) (1953) 2104–2106 (in Russian).
[7] L.G. Smith, Rev. Sci. Instrum. 23 (1) (1952) 167.
[8] L.G. Smith, Rev. Sci. Instrum. 22 (3) (1951) 166–170.

[9] L.G. Smith, C.C. Damm, Phys. Rev. 90 (2) (1953) 324–325.
[10] L.G. Smith, C.C. Damm, Rev. Sci. Instrum. 27 (8) (1956) 638–649.
[11] W. Bleakney, Am. Phys. Teacher 4 (1936) 12.
[12] W.H. Bennett Jr., J. Appl. Phys. 21 (2) (1950) 143–149.
[13] L.G. Smith, Phys. Rev. 111 (6) (1958) 1606–1619.
[14] L.G. Smith, in: H.E. Duckworth (Ed.), Proceedings of Intern. Conf. on Nuclidic Masses, University of Toronto Press, Toronto, Canada, 1960, pp. 418–424.
[15] B.A. Mamyrin, B.N. Shustrov, Mass spectrometers with resolving power a few thousand, Zh. Tekh. Fiz. 27 (6) (1957) 1347–1356 (in Russian).
[16] B.N. Shustrov, New scheme of pulse magnetic mass spectrometer with high resolving power, Zh. Tekh. Fiz. 30 (7) (1960) 860–864 (in Russian).
[17] B.A. Mamyrin, B.N. Shustrov, High resolution mass spectrometer with two stage time-of-flight separation of ions, Pribory Tekhnika Eksperimenta 5 (1962) 135–141 (in Russian).
[18] B.A. Mamyrin, B.N. Shustrov, Measurement of residual gases mass spectrum by means of mass spectrometer with high resolving power and sensitivity, Pribory Tekhnika Eksperimenta 3 (1963) 122–125 (in Russian).
[19] B.A. Mamyrin, A.A. Frantsuzov, Resonance mass spectrometer with high resolving power, Pribory Tekhnika Eksperimenta 3 (1962) 114–119 (in Russian).
[20] B.A. Mamyrin, A.A. Frantsuzov, Sov. Phys. JETP 21 (2) (1965) 274–282.
[21] B.A. Mamyrin, A.A. Frantsuzov, in: R.C. Barber (Ed.), Proceedings of the 3rd Intern. Conf. on Atomic Masses (AMCO-3), University of Manitoba Press, Vinnipeg, Canada, 1967, pp. 427–436.
[22] B.N. Taylor, W.N. Parker, D.N. Langenberg, The Fundamental Constants and Quantum Electrodynamics, Academic Press, New York, London, 1969, p. 353.
[23] B.A. Mamyrin, N.N. Aruev, S.A. Alekseenko, Sov. Phys. JETP 36 (1) (1973) 1–9.
[24] B.A. Mamyrin, N.N. Aruev, S.A. Alekseenko, in: J.N. Sanders, A.H. Wapstra (Eds.), Proceedings of the 4th Intern. Conf. on Atomic Masses (AMCO-4), Plenum Press, London-New York, 1972, pp. 451–456.
[25] S.A. Alekseenko, N.N. Aruev, B.A. Mamyrin, Determination of magnetic field components in precision magnets, Metrologia 4 (1974) 54–62 (in Russian).
[26] E.R. Cohen, B.N. Taylor, J. Phys. Chem. Ref. Data 2 (4) (1973) 663–734.
[27] E.R. Cohen, B.N. Taylor, Rev. Mod. Phys. 59 (4) (1987) 1121–1148.
[28] L.G. Smith, in: R.C. Barber (Ed.), Proceedings of the 3rd Intern. Conf. on Atomic Masses (AMCO-3), University of Manitoba Press, Vinnipeg, Canada, 1967, pp. 811–830.
[29] L.G. Smith, Phys. Rev. C 4 (1) (1971) 22–31.
[30] L.G. Smith, in: J.N. Sanders, A.H. Wapstra (Eds.), Proceedings of the 4th Intern. Conf. on Atomic Masses (AMCO-4), Plenum Press, London, New York, 1972, pp. 164–171.
[31] A.H. Wapstra, K. Bos, Atomic Data Nucl. Data Tables 19 (3) (1977) 175–297.
[32] L.G. Smith, A.H. Wapstra, Phys. Rev. C 11 (4) (1975) 1392–1400.
[33] E. Koets, in: J.N. Sanders, A.H. Wapstra (Eds.), Proceedings of the 5th Intern. Conf. on Atomic Masses (AMCO-5), Plenum Press, London, New York, 1975, pp. 164–169.
[34] E. Koets, J. Kramer, J. Nonhebel, J.B. Le Poole, in: J.A. Nolen, W. Benenson (Eds.), Proceedings of the 6th Intern. Conf. on Atomic Masses (AMCO-6), Plenum Press, London, New York, 1979, pp. 275–279.
[35] E. Koets, J. Phys. E: Sci. Instrum. 14 (1981) 1229–1232.
[36] L.G. Smith, E. Koets, A.H. Wapstra, Phys. Lett. 102B (2–3) (1981) 114–115.
[37] E. Koets, Rev. Sci. Instrum. 59 (12) (1988) 2629.
[38] A. Coc, R. Fergeau, C. Thibault, G. Audi, M. Epherve, P. Guimhal, M. de Saint Simon, R. Touchard, in: J.A. Nolen, O. Klepner (Eds.), Proceedings of the 7th Intern. Conf. on Atomic Masses (AMCO-7), Darmstadt, Seeheim, 1984, pp. 661–666.
[39] A. Coc, R. Le Gac, M. de Saint Simon, C. Thibault, F. Touchard, Nucl. Instr. Methods Phys. Res. A271 (1988) 512–517.
[40] A. Coc, R. Fergeau, R. Grabit, M. Jacotin, J.F. Kepinski, Nucl. Instr. Methods A 305 (1) (1991) 143–149.
[41] M. de Saint Simon, C. Thibault, G. Audi, A. Coc, H. Doubre, M. Jacotin, J.F. Kepinski, R. Le Gac, G. Le Scornet, Phys. Scripta 59 (1995) 406–409.
[42] C. Thibault, A. Coc, R. Fergeau, R. Le Gac, M. De Saint Simon, R. Touchard, in: K. Conrad, K. Eberhard (Eds.), 9th European Symposium on Antiproton–Proton Interaction and Fundamental Symmetries, Mainz, Germany, 1989, pp. 454–456.
[43] C. Thibault, A. Coc, R. Fergeau, R. Le Gac, M. de Saint Simon, F. Touchard, E. Haebel, H. Herr, R. Klapisch, G. Lebee, G. Petrucci, G. Stefanini, Nucl Phys. B (Proceedings Supplements) 8 (1989) 454–456.
[44] D. Lunney, G. Audi, H. Doubre, S. Henry, M. de Saint Simon, C. Thibault, Phys. Rev. C 64 (5) (2001) 054311 (12).
[45] C. Gaulard, G. Audi, C. Bachelet, D. Lunney, M. de Saint Simon, C. Thibault, N. Vieira, Nucl. Phys. A 766 (2006) 52–73.
[46] D. Lunney, G. Audi, C. Gaulard, M. De Saint Simon, C. Thibault, N. Vieira, Eur. Phys. J. A 28 (2006) 129–138.
[47] C. Bachelet, G. Audi, C. Gaulard, C. Guenaut, F. Herfurth, D. Lunney, M. de Saint Simon, C. Thibault, Phys. Rev. Lett. 100 (18) (2008) 182501 (4).
[48] G.S. Anufriev, B.A. Mamyrin, The measurement of magnetic field inhomogeneities with high accuracy, Pribory Tekhnika Eksperimenta 4 (1968) 195–198 (in Russian).
[49] N.N. Aruev, E.L. Baidakov, B.A. Mamyrin, A.V. Yakovlev, Sov. J. Tech. Phys. 33 (3) (1988) 321–324.
[50] N.N. Aruev, E.L. Baidakov, J. Tech. Phys. 40 (4) (1995) 385–387.
[51] B.A. Mamyrin, I.N. Tolstikhin, G.S. Anufriev, I.L. Kamensky, The usage of a magnetic resonance mass spectrometerfor isotopic analyses of primordial helium, Geokhimiya 5 (1969) 595–602 (in Russian).
[52] B.A. Mamyrin, B.N. Shustrov, G.S. Anufriev, B.S. Boltenkov, V.A. Zagulin, I.L. Kamensky, I.N. Tolstikhin, L.V. Khabarin, The measurement of helium isotopes by means of magnetic resonance mass spectrometer, Zh. Tekh. Fiz. 42 (12) (1972) 2577–2584 (in Russian).
[53] I.L. Kamensky, V.P. Yakutseni, B.A. Mamyrin, G.S. Anufriev, I.N. Tolstikhin, Helium isotopes in nature, Geokhimiya 8 (1971) 914–931 (in Russian).
[54] B.A. Mamyrin, G.S. Anufriev, I.L. Kamensky, I.N. Tolstikhin, Isotope composition of atmospheric helium, Dokl. Akad. Nauk SSSR 195 (1970) 111 (in Russian).
[55] B.A. Mamyrin, G.S. Anufriev, I.L. Kamensky, I.N. Tolstikhin, The determination of atmospheric helium isotope composition, Geokhimiya 6 (1970) 721–730 (in Russian).
[56] B.K. Alekseichuk, G.S. Anufriev, G.I. Afonina, B.S. Boltenkov, B.A. Mamyrin, Mass spectrometer MI-9302 for analyses of small amounts of inert and chemically active gases, Pribory Tekhnika Eksperimenta 4 (1979) 206–209 (in Russian).
[57] G.S. Anufriev, B.S. Boltenkov, B.A. Mamyrin, The possibilityof using of titanium alloys for manufacturing of mass spectrometric analyzers, Pribory Tekhnika Eksperimenta 1 (1982) 160–163 (in Russian).
[58] G.S. Anufriev, G.I. Afonina, B.A. Mamyrin, V.T. Nenarokomova, A.E. Rafalson, Operation of the mass spectrometer MI-9302 in static pump mode, Pribory Tekhnika Eksperimenta 4 (1979) 211–213 (in Russian).
[59] B.A. Mamyrin, I.N. Tolstikhin, G.S. Anufriev, I.L. Kamensky, Anomalous isotopic composition of helium in volcanic gases, Dokl. Akad. Nauk SSSR 184 (5) (1969) 1197–1199 (in Russian).
[60] B.A. Mamyrin, I.N. Tolstikhin, G.S. Anufriev, I.L. Kamensky, Isotope composition of helium in Icelandic hot springs, Geokhimiya 11 (1972) 1936 (in Russian).
[61] I.S. Lomonosov, B.A. Mamyrin, E.M. Prasolov, I.N. Tolstikhin, Isotope composition of helium and argon in hot springs of Baikal rift zone, Geokhimiya 11 (1976) 1743–1746 (in Russian).
[62] V.I. Kononov, B.G. Polyak, B.A. Mamyrin, L.V. Khabarin, The helium isotopes in the Icelandic hydrothemae, Dokl. Akad. Nauk SSSR 217 (1) (1974) 172–175 (in Russian).
[63] B.G. Polyak, E.M. Prasolov, G.I. Buachidze, V.I. Kononov, B.A. Mamyrin, L.V. Khabarin, Isotope composition of He and Ar in fluids of the Alpine-Apennine region and its relation with volcanic activity, Dokl. Akad. Nauk. SSSR 247 (6) (1979) 1220–1225 (in Russian).
[64] O.V. Klyavin, B.A. Mamyrin, L.V. Khabarin, Yu. M. Chernov, V.S. Yudenich, Helium penetration in LiF crystals by their deformation in liquid ^{4}He and ^{3}He, Fizika Tverdogo Tela 18 (1976) 1281–1285.
[65] O.V. Klyavin, B.A. Mamyrin, L.V. Khabarin, Yu.M. Chernov, V.S. Yudenich, Dynamic diffusion of helium into various type of solids during their deformation and dispersion, Phys. Solid State 47 (5) (2005) 863–868.
[66] G.S. Anufriev, B.S. Boltenkov, V.N. Gartmanov, V.N. Gartmanov, G.E. Kocharov, B.A. Mamyrin, V.P. Pavlov, Helium, neon, argon in the lunar soil from Mare Fertility, Geokhimiya 8 (1977) 1129–1135 (in Russian).
[67] G.S Anufriev, B.S. Boltenkov, Doklady Earth Sci. 405 (8) (2005) 1205–1208.
[68] G.S. Anufriev, B.S. Boltenkov, I.N. Kapitonov, XX Lunar and Planetary Science Conference, 13–17 March, 1989, No. 1010.
[69] G.S. Anufriev, L.N. Blinov, B.S. Boltenkov, M. Arif, Tech. Phys. 50 (5) (2005) 663–665.
[70] G.S. Anufriev, B.S. Boltenkov, A.I. Ryabinkov, Tech. Phys. 51 (1) (2006) 100–111.
[71] Yu.A. Akulov, N.N. Aruev, B.A. Mamyrin, V.S. Yudenich, The method of tritium half life determination, Bull. Invent. 4 (1988) 265 (in Russian).
[72] Yu.A. Akulov, B.A. Mamyrin, L.V. Khabarin, V.S. Yudenich, N.N. Ryazantseva, Sov. Tech. Phys. Lett. 14 (5) (1988) 416.
[73] Yu.A. Akulov, B.A. Mamyrin, Phys. Lett. B 600 (2004) 41–47.
[74] G.S. Anufriev, V.N. Gartmanov, B.A. Mamyrin, V.P. Pavlov, A vacuum extracting system with low background, Pribory Tekhnika Eksperimenta 1 (1977) 248–250 (in Russian).
[75] B.A. Mamyrin, L.V. Khabarin, Manifold metal furnace for inert gas extraction, Pribory Tekhnika Eksperimenta 2 (1977) 232–233 (in Russian).
[76] N.N. Aruev, B.S. Boltenkov, Tech. Phys. Lett. 36 (4) (2010) 337–340.
[77] Yu.A. Akulov, B.A. Mamyrin, L.V. Khabarin, V.S. Yudenich, The increasing of isotopic sensitivity of magnetic resonance mass spectrometer, Pribory Tekhnika Eksperimenta 2 (1985) 173–175 (in Russian).
[78] B.A. Mamyrin, I.N. Tolstikhin, Helium Isotopes in Nature, Elsevier, Amsterdam, Oxford, New York, Tokyo, 1984, p. 273.
[79] B.A. Mamyrin, S.A. Alekseenko, N.N. Aruev, Sov. Phys. JETP 53 (6) (1981) 1109–1112.
[80] N.N. Aruev, E.L. Baidakov, B.A. Mamyrin, Sov. J. Tech. Phys. 32 (2) (1987) 180–183.
[81] N.N. Aruev, E.L. Baidakov, B.A. Mamyrin, A.V. Yakovlev, Sov. J. Tech. Phys. 32 (3) (1987) 303–308.
[82] N.N. Aruev, E.L. Baidakov, Tech. Phys. 44 (4) (1999) 431–437.
[83] N.N. Aruev, E.L. Baidakov, B.A. Mamyrin, Tech. Phys. 52 (2) (2007) 258–262.